Chapter 8
Time-Frequency Analysis

Fourier-analysis provides a description of a given data set in terms of monochromatic oscillations without any time information. It is thus mostly useful for stationary signals. If the spectrum changes in time it is desirable to obtain information about the time at which certain frequencies appear. This can be achieved by applying Fourier analysis to a short slice of the data (short time Fourier analysis) which is shifted along the time axis. The frequency resolution is the same for all frequencies and therefore it can be difficult to find a compromise between time and frequency resolution. Wavelet analysis uses a frequency dependent window and keeps the relative frequency resolution constant. This is achieved by scaling and shifting a prototype wavelet - the so called mother wavelet. Depending on the application wavelets can be more general and need not be sinusoidal or even continuous functions. Multiresolution analysis provides orthonormal wavelet bases which simplify the wavelet analysis. The fast wavelet transform connects a set of sampled data with its wavelet coefficients and is very useful for processing audio and image data.

8.1 Short Time Fourier Transform (STFT)

Fourier analysis transforms a function in the time domain $f(t)$ into its spectrum

$$\widetilde{f}(\omega) = \mathcal{F}[f](\omega) = \frac{1}{\sqrt{2\pi}} \int_{-\infty}^{\infty} f(t) \mathrm{e}^{-\mathrm{i}\omega t} dt \tag{8.1}$$

thereby losing all time information. Short time Fourier analysis applies a windowing function[1] (p. 133) e.g. a simple rectangle (Fig. 8.1)[2]

[1] Also known as apodization function or tapering function.

[2] There are two different definitions of the sinc function in the literature.

P.O.J. Scherer, *Computational Physics*, Graduate Texts in Physics,
DOI 10.1007/978-3-319-61088-7_8

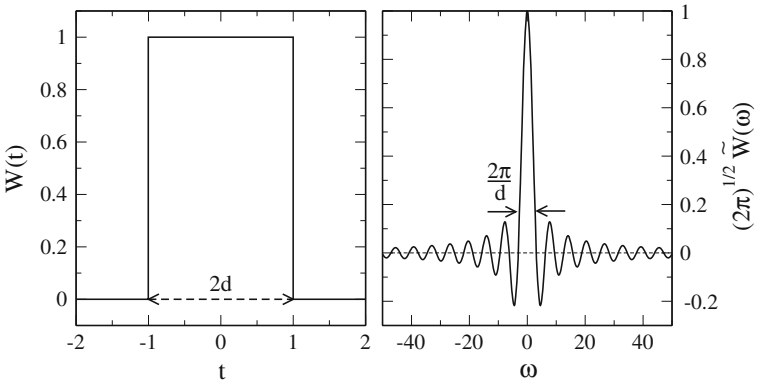

Fig. 8.1 (Rectangular window) The rectangular (uniform) window and its Fourier transform are shown for $d = 1$

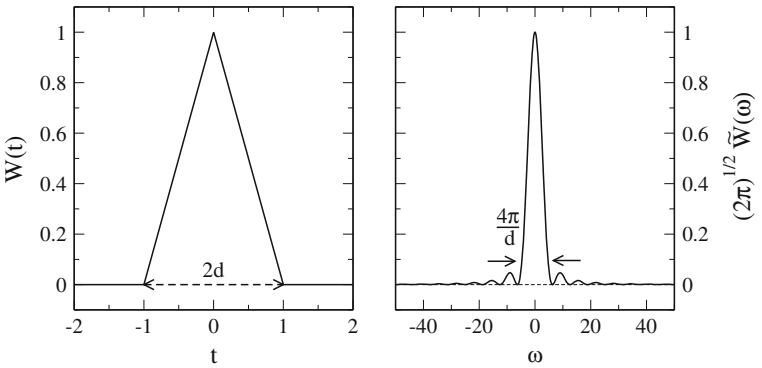

Fig. 8.2 (Triangular window) The *triangular* (Bartlett) window and its Fourier transform are shown for $d = 1$

$$W_R(t) = \begin{cases} 1 \text{ for } |t| \leq d \\ 0 \text{ else} \end{cases} \tag{8.2}$$

$$\tilde{W_R}(\omega) = \frac{2d}{\sqrt{2\pi}} \frac{\sin \omega d}{\omega d} = \frac{2d}{\sqrt{2\pi}} \text{sinc}(\omega d) \tag{8.3}$$

or triangle (Fig. 8.2)

$$W_{Tr}(t) = \begin{cases} \left(1 - \frac{|t|}{d}\right) \text{ for } t \leq d \\ 0 \text{ else} \end{cases} \tag{8.4}$$

$$\tilde{W}_{Tr}(\omega) = \frac{d}{\sqrt{2\pi}} \frac{2(1 - \cos \omega d)}{\omega^2 d^2} == \frac{d}{\sqrt{2\pi}} \left(\text{sinc}\left(\frac{\omega d}{2}\right)\right)^2. \tag{8.5}$$

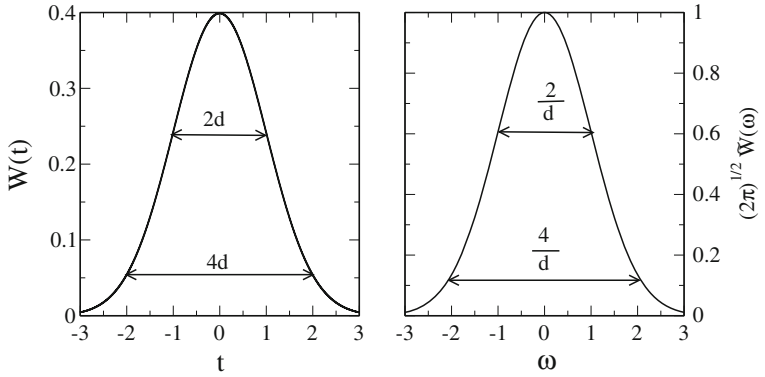

Fig. 8.3 (Gaussian window) The Gaussian window and its Fourier transform are shown for $d = 1$

A smoother window is the Gaussian (p. 192) (Fig. 8.3)

$$W_G(t) = \frac{1}{d\sqrt{2\pi}} \exp\left\{-\frac{t^2}{2d^2}\right\} \tag{8.6}$$

with

$$\tilde{W}_G(\omega) = \frac{1}{\sqrt{2\pi}} \exp\left\{-\frac{\omega^2 d^2}{2}\right\}. \tag{8.7}$$

For the Gaussian window the standard deviations[3]

$$\sigma_t = d \quad \sigma_\omega = \frac{1}{d} \tag{8.8}$$

obey the uncertainty relation[4]

$$\sigma_t \sigma_\omega = 1. \tag{8.9}$$

Since the Gaussian extends to infinity, it has to be cut off for practical calculations.

Quite popular are the Hann(ing) and Hamming windows (Fig. 8.4)

$$W_{Hann}(t) = \cos^2\left(\frac{\pi t}{2d}\right) = \left(\frac{1}{2} + \frac{1}{2}\cos\frac{\pi t}{d}\right) \tag{8.10}$$

[3]Here we use the definition $\sigma^2 = \int_{-\infty}^{\infty} dt\, W(t)t^2$. If instead $\sigma^2 = \int_{-\infty}^{\infty} dt\, |W(t)|^2 t^2$ is used then $\sigma_t = \frac{d}{\sqrt{2}}$ and $\sigma_\omega = \frac{1}{\sqrt{2}d}$.

[4]For a Gaussian the time-bandwidth product is minimal.

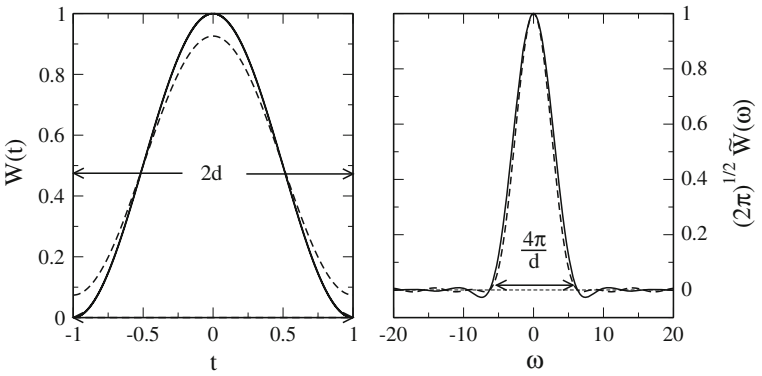

Fig. 8.4 (Hann and Hamming window) The Hann (*full curves*) and Hamming (*dashed curves*) windows together with their Fourier transforms are shown for $\Delta t = 1$. The Hamming window is optimized to reduce the side lobes in the spectrum

$$\tilde{W}_{Hann}(\omega) = \frac{d}{\sqrt{2\pi}} \frac{\mathrm{sinc}\omega d}{1 - \frac{\omega^2 d^2}{\pi^2}} \tag{8.11}$$

$$W_{Hamm}(t) = \left(\frac{27}{54} + \frac{23}{54}\cos\frac{\pi t}{d}\right) \tag{8.12}$$

$$\tilde{W}_{Hamm}(\omega) = \frac{d}{\sqrt{2\pi}} \frac{1 - \frac{4}{27}\frac{\omega^2 d^2}{\pi^2}}{1 - \frac{\omega^2 d^2}{\pi^2}} \mathrm{sinc}\omega d. \tag{8.13}$$

For a general real valued function

$$\tilde{W}(\omega)^* = \left(\frac{1}{\sqrt{2\pi}} \int_{-\infty}^{\infty} W(t) \mathrm{e}^{-\mathrm{i}\omega t} dt\right)^* = \frac{1}{\sqrt{2\pi}} \int_{-\infty}^{\infty} W(t) \mathrm{e}^{\mathrm{i}\omega t} dt = \tilde{W}(-\omega) \tag{8.14}$$

and for an even function

$$\tilde{W}(\omega) = \frac{1}{\sqrt{2\pi}} \int_{-\infty}^{\infty} W(t) \mathrm{e}^{-\mathrm{i}\omega t} dt = \frac{1}{\sqrt{2\pi}} \int_{\infty}^{-\infty} W(t) \mathrm{e}^{\mathrm{i}\omega t} d(-t) = \tilde{W}(-\omega). \tag{8.15}$$

If $W(t)$ is real and even than this holds also for its Fourier transform

$$\tilde{W}(-\omega) = \tilde{W}(\omega) = \tilde{W}(\omega)^* = \frac{1}{\sqrt{2\pi}} \int_{-\infty}^{\infty} W(t) \cos(\omega t) dt. \tag{8.16}$$

The short time Fourier Transform

$$X(t_0, \omega) = \mathcal{F}[W^*(t - t_0) f(t)](\omega) = \frac{1}{\sqrt{2\pi}} \int_{-\infty}^{\infty} W^*(t - t_0) f(t) \mathrm{e}^{-\mathrm{i}\omega t} dt \tag{8.17}$$

depends on two variables t_0 and ω. Since it has the form of a convolution integral it becomes a product in Fourier space, where

$$\begin{aligned}
&\frac{1}{\sqrt{2\pi}} \int dt_0 \mathrm{e}^{-\mathrm{i}\omega_0 t_0} X(t_0, \omega) = \frac{1}{\sqrt{2\pi}} \int_{-\infty}^{\infty} dt_0 \mathrm{e}^{-\mathrm{i}\omega_0 t_0} \frac{1}{\sqrt{2\pi}} \int_{-\infty}^{\infty} dt \; W^*(t - t_0) f(t) \mathrm{e}^{-\mathrm{i}\omega t} \\
&= \frac{1}{2\pi} \int_{-\infty}^{\infty} \int_{-\infty}^{\infty} dt \, d(t - t_0) \mathrm{e}^{\mathrm{i}\omega_0 (t - t_0)} \; W^*(t - t_0) f(t) \mathrm{e}^{-\mathrm{i}\omega_0 t} \mathrm{e}^{-\mathrm{i}\omega t} \\
&= \frac{1}{2\pi} \left(\int_{-\infty}^{\infty} d(t - t_0) \mathrm{e}^{-\mathrm{i}\omega_0 (t - t_0)} W(t - t_0) \int_{-\infty}^{\infty} \right)^* dt \;\; f(t) \mathrm{e}^{-\mathrm{i}\omega_0 t} \mathrm{e}^{-\mathrm{i}\omega t} \\
&= \tilde{W}^*(\omega_0) \tilde{f}(\omega + \omega_0).
\end{aligned} \tag{8.18}$$

For a real valued an even windowing function like the Gaussian (8.6) the STFT can therefore be calculated from

$$X(t_0, \omega) = \frac{1}{\sqrt{2\pi}} \int d\omega_0 \mathrm{e}^{\mathrm{i}\omega_0 t_0} \tilde{W}(\omega_0) \tilde{f}(\omega_0 + \omega). \tag{8.19}$$

Alternatively, the STFT can be formulated as

$$X(t_0, \omega) = \frac{1}{\sqrt{2\pi}} \mathrm{e}^{\mathrm{i}\omega t_0} \int_{-\infty}^{\infty} f(t) \; W^*(t - t_0) \mathrm{e}^{-\mathrm{i}\omega (t - t_0)} dt \tag{8.20}$$

$$= \frac{1}{\sqrt{2\pi}} \mathrm{e}^{\mathrm{i}\omega t_0} \int_{-\infty}^{\infty} f(t) \; \Omega^*(t - t_0) dt$$

which involves a convolution of $f(t)$ with the wave packet (Fig. 8.5)

$$\Omega(t - t_0) = W(t - t_0) \mathrm{e}^{\mathrm{i}\omega (t - t_0)} \tag{8.21}$$

which is localized around t_0. In frequency space the wave packet becomes a band pass filter

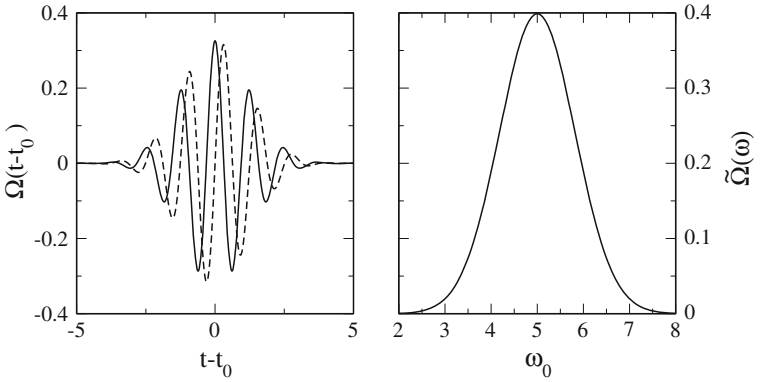

Fig. 8.5 (Gabor wave packet) ***Left*** Real (*full curve*) and imaginary (*dashed curve*) part of the wave packet (8.21) are shown for a Gaussian windowing function with $\omega = 5$ and $2d^2 = 3$. ***Right*** In the frequency domain the wave packet acts as a bandpass filter at $\omega_0 = \omega$

$$\begin{aligned}
&\tilde{\Omega}(\omega_0) = \frac{1}{\sqrt{2\pi}} \int_{-\infty}^{\infty} dt \mathrm{e}^{-\mathrm{i}\omega_0 t} W(t) \mathrm{e}^{\mathrm{i}\omega t} \\
&= \frac{1}{\sqrt{2\pi}} \int_{-\infty}^{\infty} dt \mathrm{e}^{-\mathrm{i}(\omega_0-\omega)t} W(t) \\
&= \tilde{W}(\omega_0 - \omega)
\end{aligned}$$

$$\begin{aligned}
&\frac{1}{2\pi} \int_{-\infty}^{\infty} dt_0 \mathrm{e}^{-\mathrm{i}\omega_0 t_0} \int_{-\infty}^{\infty} f(t)\, \Omega^*(t - t_0) dt \\
&= \frac{1}{2\pi} \int_{-\infty}^{\infty} dt \int_{-\infty}^{\infty} d(t - t_0)\, f(t) \mathrm{e}^{-\mathrm{i}\omega_0 t}\, \Omega^*(t - t_0) \mathrm{e}^{\mathrm{i}\omega_0 (t-t_0)} \\
&= \tilde{f}(\omega_0) \tilde{\Omega}^*(\omega_0)
\end{aligned} \tag{8.22}$$

$$\begin{aligned}
&X(t_0, \omega) = \frac{1}{\sqrt{2\pi}} \mathrm{e}^{\mathrm{i}\omega t_0} \int_{-\infty}^{\infty} d\omega_0 \mathrm{e}^{\mathrm{i}\omega_0 t_0} \tilde{f}(\omega_0) \tilde{\Omega}^*(\omega_0) \\
&= \frac{1}{\sqrt{2\pi}} \int_{-\infty}^{\infty} d\omega_0 \mathrm{e}^{\mathrm{i}(\omega+\omega_0)t_0} \tilde{f}(\omega_0) \tilde{\Omega}^*(\omega_0) \\
&= \frac{1}{\sqrt{2\pi}} \int_{-\infty}^{\infty} d\omega_0 \mathrm{e}^{\mathrm{i}\omega t_0} \tilde{f}(\omega_0 - \omega) \tilde{\Omega}^*(\omega_0 - \omega).
\end{aligned}$$

The STFT can be inverted by

$$\int d\omega X(t_0,\omega)\mathrm{e}^{\mathrm{i}\omega t_0} = \frac{1}{\sqrt{2\pi}}\int dt \int d\omega \mathrm{e}^{\mathrm{i}\omega t_0} W^*(t-t_0) f(t)\mathrm{e}^{-\mathrm{i}\omega t}$$
$$= \frac{1}{\sqrt{2\pi}}\int dt W^*(t-t_0) f(t) 2\pi\delta(t-t_0) = \sqrt{2\pi} W^*(0) f(t_0) \tag{8.23}$$

or alternatively

$$\int dt_0 \int d\omega X(t_0,\omega)\mathrm{e}^{\mathrm{i}\omega t} = \int dt_0 \int d\omega \frac{1}{\sqrt{2\pi}}\mathrm{e}^{\mathrm{i}\omega t}\int_{-\infty}^{\infty} W^*(t'-t_0) f(t')\mathrm{e}^{-\mathrm{i}\omega t'} dt'$$
$$= \int dt_0 \frac{1}{\sqrt{2\pi}}\int_{-\infty}^{\infty} 2\pi\delta(t-t') W^*(t'-t_0) f(t') dt'$$
$$= \int dt_0 \frac{1}{\sqrt{2\pi}} 2\pi W^*(t-t_0) f(t) = \sqrt{2\pi} f(t)\int W^*(t') dt'. \tag{8.24}$$

STFT with a Gaussian window is also known as Gabor transform [79] which is conventionally defined as

$$\mathcal{G}[f](t_0,\omega) = \int_{-\infty}^{\infty} dt\, \mathrm{e}^{-\alpha\pi(t-t_0)^2}\mathrm{e}^{-\mathrm{i}\omega t} f(t). \tag{8.25}$$

Example: Spectrogram

The STFT is often used to analyze audio signals. Let us consider as a simple example a monochromatic signal, which is switched on at time $t = 0$

$$f(t) = \begin{cases} 0 & t < 0 \\ \sin(\omega_s t) & t \geq 0. \end{cases} \tag{8.26}$$

Using a Gaussian window, the Fourier transform can be calculated explicitly (an algebra program is very helpful)

$$X(t_0,\omega) = \frac{1}{2\pi\Delta t}\int_0^{\infty} dt\, \mathrm{e}^{-\mathrm{i}\omega t}\mathrm{e}^{-(t-t_0)^2/2d^2}\sin(\omega_s t)$$
$$= -\frac{\mathrm{i}}{4\sqrt{2\pi}}\mathrm{e}^{-\mathrm{i}t_0(\omega-\omega_s)}\mathrm{e}^{-d^2(\omega-\omega_s)^2/2}\left(\mathrm{erf}\left(\frac{\mathrm{i}\Delta t^2(\omega-\omega_s)-t_0}{\sqrt{2}d}\right)-1\right)$$
$$+\frac{\mathrm{i}}{4\sqrt{2\pi}}\mathrm{e}^{-\mathrm{i}t_0(\omega+\omega_s)}\mathrm{e}^{-d^2(\omega+\omega_s)^2/2}\left(\mathrm{erf}\left(\frac{\mathrm{i}d^2(\omega+\omega_s)-t_0}{\sqrt{2}d}\right)-1\right). \tag{8.27}$$

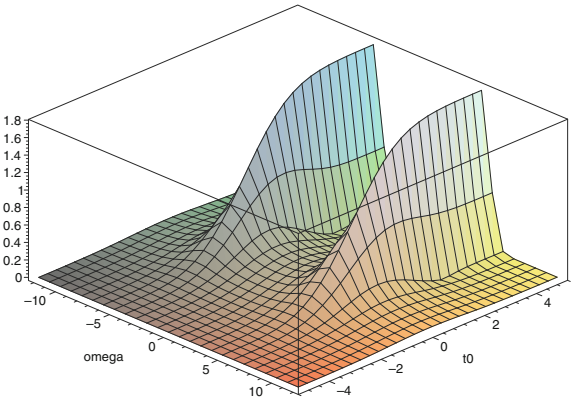

Fig. 8.6 (3-d spectrogram) The squared magnitude of the STFT (8.27) is shown for $\omega_s = 5$ and $2d = 1$

There are two contributions since the real function $f(t)$ contains oscillations with $\pm\omega_s$. The squared magnitude[5] $|X(t_0, \omega)|^2$ is shown as a 3-d spectrogram in Fig. 8.6. The width of the window determines the resolution both in time and frequency. Neglecting interference terms, at resonance $\omega = \omega_s$ the squared magnitude rises according to

$$|X(t_0, \omega_s)|^2 = \frac{1}{32\pi}\left(\text{erf}\,\frac{t_0}{\sqrt{2}d} - 1\right)^2 \tag{8.28}$$

and reaches its stationary value within a time of $\approx 2d$, whereas in the stationary state at $t_0 \gg d$, the dependency on the frequency mismatch $\Delta\omega = \omega - \omega_s$ is given by a Gaussian with a width of $2\sigma_\omega = \sqrt{2}/d$. The dependence of time and frequency resolution on the window width is shown qualitatively by 2-dimensional spectrograms in Fig. 8.7.

8.2 Discrete Short Time Fourier Transform

The continuous STFT is very redundant and not useful for the analysis of data which are sampled at discrete times. Therefore we introduce a series of overlapping windows centered at equidistant times $t_n = n\Delta t$ (Fig. 8.8)

$$W_n(t) = W(n\Delta t - t). \tag{8.29}$$

[5] This is a measure of the spectral power distribution.

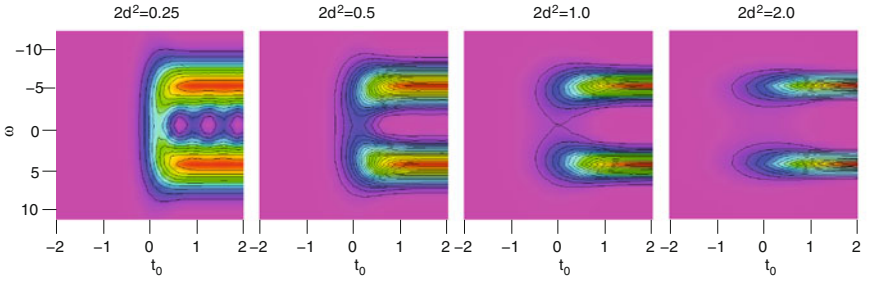

Fig. 8.7 (Spectrograms with different window width Δt) The squared magnitude of the STFT (8.27) is shown for $\omega_s = 5$ and $2d^2 = 0.25, 0.5, 1.0, 2.0$. For larger values of the time window d the frequency resolution becomes higher but the time resolution lower

Assuming that the windowing function $W_n(t) = 0$ outside the interval $[t_n - d, t_n + d]$ we apply (7.5) and expand $W_n(t) f(t)$ inside the interval as a Fourier series

$$g_n(t) = W_n(t) f(t) = \sum_{m=-\infty}^{\infty} \mathrm{e}^{\mathrm{i}\omega_m t} \hat{g}_{nm} \text{ with } \omega_m = m\frac{\pi}{d} \quad |t - t_n| \le d. \tag{8.30}$$

We extend this expression to all times t by introducing the characteristic function of the interval

$$\chi_n(t) = \begin{cases} 1 & \text{for } |t - t_n| \le d \\ 0 & \text{else} \end{cases} \tag{8.31}$$

$$g_n(t) = W_n(t) f(t) = \chi_n(t) \sum_{m=-\infty}^{\infty} \mathrm{e}^{\mathrm{i}\omega_m t} \hat{g}_{nm}. \tag{8.32}$$

The Fourier coefficients, given by the integral

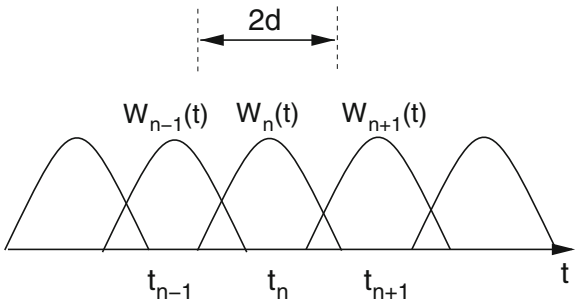

Fig. 8.8 (Discrete STFT) Assuming that the windowing function $W_n(t) = 0$ outside the interval $[t_n - d, t_n + d]$ we apply (7.5) and expand $W_n(t) f(t)$ inside the interval as a Fourier series

$$\hat{g}_{nm} = \frac{1}{2d} \int_{t_n-d}^{t_n+d} W(t - t_n) f(t) \mathrm{e}^{-\mathrm{i}\omega_m t} dt \tag{8.33}$$

obviously correspond to the STFT at times t_n and frequencies ω_m

$$X(t_n, \omega_m) = \frac{1}{\sqrt{2\pi}} \int_{-\infty}^{\infty} W(t - t_n) f(t) \mathrm{e}^{-\mathrm{i}\omega_m t} dt = \frac{1}{\sqrt{2\pi}} \int_{t_n-d}^{t_n+d} W(t - t_n) f(t) \mathrm{e}^{-\mathrm{i}\omega_m t} dt$$
$$= \frac{2d}{\sqrt{2\pi}} \hat{g}_{nm}. \tag{8.34}$$

If the windows are dense enough such that there union spans all times, the signal can be reconstructed by summation

$$\sum_n g_n(t) = f(t) \sum_n W_n(t) = \sum_{nm} \chi_n(t) \mathrm{e}^{\mathrm{i}\omega_m t} \hat{g}_{nm}. \tag{8.35}$$

This expression simplifies, if

$$\sum_n W_n(t) = \text{const} \tag{8.36}$$

which is e.g. the case for triangular windows as well as the Hann and Hamming windows with $\Delta t = d$ (Fig. 8.9).

For practical applications, we assume that the function $g(t)$ has been sampled at N equidistant times within the interval $[t_n - d, t_n + d]$

$$\tau_{n,s} = t_n - d + s\frac{2d}{N} \quad s = 0, 1, \ldots N - 1 \tag{8.37}$$

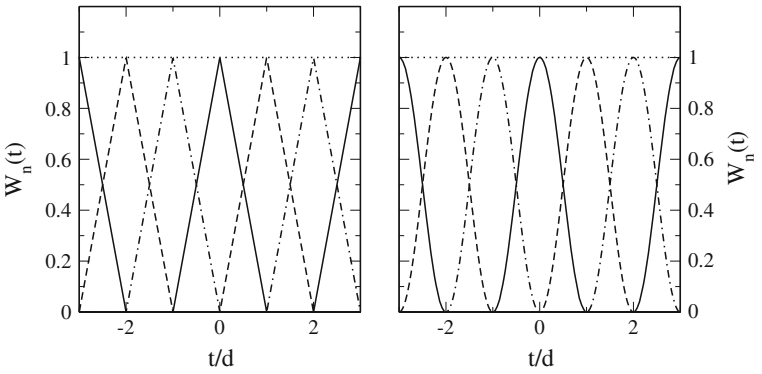

Fig. 8.9 (Window functions with constant sum) For the triangular (***Left***) and the Hann and Hamming (***Right***) window the sum $\sum_n W_n(t)$ becomes constant (*dotted lines*) if the windows are shifted by half their width $\Delta t = d$

$$\omega_j = \frac{\pi}{d} j, \quad \omega_j(\tau_{n,s} - t_n + d) = js\frac{2\pi}{N} \tag{8.38}$$

and apply the discrete Fourier transformation method (p. 131)

$$\widetilde{g}_{n,\omega_j} = \sum_{s=0}^{N-1} g_{n,s} \mathrm{e}^{-\mathrm{i}\omega_j(\tau_{ns} - t_n + d)} = \sum_{s=0}^{N-1} g_{n,s} \mathrm{e}^{-\mathrm{i}js\frac{2\pi}{N}} \tag{8.39}$$

$$\frac{1}{N}\sum_{j=0}^{N-1} \tilde{g}_{n,\omega_j} \mathrm{e}^{\mathrm{i}js\frac{2\pi}{N}} = \frac{1}{N}\sum_{j=0}^{N-1}\sum_{s=0}^{N-1} g_{n,s'} \mathrm{e}^{-\mathrm{i}js'\frac{2\pi}{N}} \mathrm{e}^{\mathrm{i}js\frac{2\pi}{N}} = g_{n,s}. \tag{8.40}$$

Example: FM Signal

Figures 8.10 and 8.11 show the STFT analysis of a frequency modulated signal

$$f(t) = \sin\Phi(t) = \sin\left(\omega_0 t + \frac{a\omega_0}{\omega_1}(1 - \cos\omega_1 t)\right) \tag{8.41}$$

with a momentaneous frequency of

$$\omega(t) = \frac{\partial\Phi}{\partial t} = \omega_0(1 + a\sin\omega_1 t) \tag{8.42}$$

for carrier frequency $\frac{\omega_0}{2\pi} = 10\,\mathrm{kHz}$, modulation frequency $\frac{\omega_1}{2\pi} = 25\,\mathrm{Hz}(100\,\mathrm{Hz})$ and modulation depth $a = 0.3$.

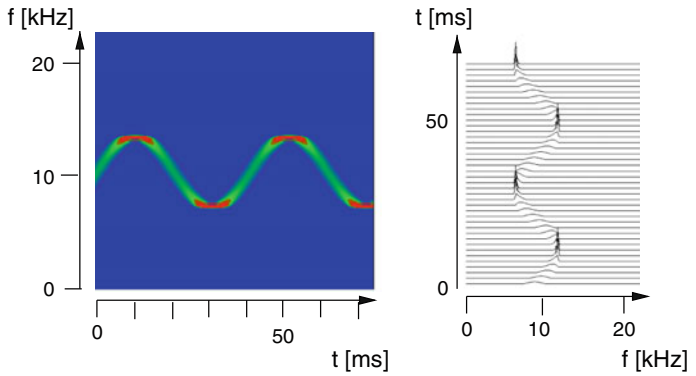

Fig. 8.10 (STFT analysis of a FM signal) The figure shows screenshots from Problem 8.1. ***Left*** spectrogram ***Right*** STFT spectra. Sampling frequency is 44100 Hz, number of samples 512, Hann windows are used with a shift of 8 samples (0.18 ms) between neighbor windows. 6 ms time resolution and 1.1 kHz frequency resolution are sufficient to resolve the 25 Hz modulation. The time dependent spectra have their smallest width at the stationary points of the momentaneous frequency

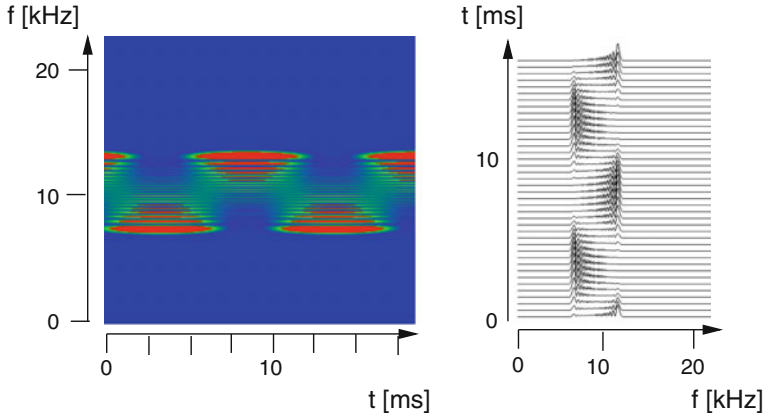

Fig. 8.11 (STFT analysis of a FM signal) The figure shows screenshots from Problem 8.1. ***Left*** spectrogram ***Right*** STFT spectra. Sampling frequency is 44100 Hz, number of samples 512, Hann windows are used with a shift of 2 samples (0.045 ms) between neighbor windows. 6 ms time resolution and 1.1 kHz frequency resolution are not sufficient to resolve the 100 Hz modulation. Only minimum and maximum frequencies are observed

8.3 Gabor Expansion

For the special case of rectangular windows with distance $\Delta t = 2d$[6]

$$W_n(t) = W_R(t - 2d\,n) = \chi_n(t) \tag{8.43}$$

$$\sum_n W_n(t) = 1 = \text{const} \tag{8.44}$$

we have

$$f(t) = \sum_n g_n(t) \tag{8.45}$$

$$= \sum_n \sum_{m=-\infty}^{\infty} \chi_n(t) \mathrm{e}^{\mathrm{i}\omega_m t} \hat{g}_{nm}. \tag{8.46}$$

This equation expands $f(t)$ and its Fourier transform as linear combinations of elementary "signals" which are located at t_n in time and ω_m in frequency

$$h_{n,m} = \chi_n \mathrm{e}^{\mathrm{i}\omega_m t}. \tag{8.47}$$

[6]For simplicity, we do not normalize the window here.

$$\tilde{h}_{n,m} = \frac{2d}{\sqrt{2\pi}} \mathrm{e}^{-\mathrm{i}t_n(\omega-\omega_m)} \operatorname{sinc} d(\omega - \omega_m) \tag{8.48}$$

$$f(t) = \sum_{nm} h_{n,m}\hat{g}_{n,m} \quad \tilde{f}(\omega) = \sum_{nm} \tilde{h}_{nm}\hat{g}_{nm}. \tag{8.49}$$

A similar expansion is obtained if we use rectangular windows in Fourier space with width and distance $\Delta\omega$ [80]

$$\tilde{h}_{nm}(\omega) = \chi_{\mathrm{m}} \mathrm{e}^{-\mathrm{i}t_n(\omega-\omega_m)}$$

$$h_{nm}(t) = \frac{2\Delta\omega}{\sqrt{2\pi}} \operatorname{sinc}((t - t_n)\Delta\omega)\mathrm{e}^{\mathrm{i}\omega_m t}$$

and sample the spectrum at times

$$t_n = n\frac{\pi}{\Delta\omega} \tag{8.50}$$

to obtain

$$\tilde{f}(\omega) = \sum \chi_m(\omega)\tilde{f}_m(\omega) = \sum_{n=-\infty}^{\infty} \chi_m(\omega)\mathrm{e}^{\mathrm{i}\omega t_n} \hat{f}_{nm} \tag{8.51}$$

$$\hat{f}_{nm} = \frac{1}{2\Delta\omega} \int_{\omega_m-\Delta\omega}^{\omega_m+\Delta\omega} \tilde{f}(\omega)\mathrm{e}^{\mathrm{i}\omega t_n} d\omega. \tag{8.52}$$

Gabor [79] discussed an expansion with Gaussian signals (Fig. 8.5). In general, however, the elementary signals are not orthogonal which makes the determination of the coefficients $a_{n,m}$ complicated. Bastiaans [80, 81] introduced another auxiliary set of elementary signals

$$\gamma_{n,m} = \gamma(t - n\Delta t)\mathrm{e}^{\mathrm{i}\omega_m t} \tag{8.53}$$

which are biorthogonal, i.e.

$$\int \gamma^*_{n',m'}(t)h_{n,m}(t)dt = \delta_{n,n'}\delta_{m,m'} \tag{8.54}$$

and allow the calculation of the Gabor expansion coefficients from a scalar product

$$\int \gamma^*_{n,m}(t)f(t)dt = \sum_{nm} \int a_{nm}\gamma^*_{n,m}h_{nm}(t)dt = a_{nm}. \tag{8.55}$$

Determination of γ for a given windowing function can be simplified by application of the Zak transform [82]. Discrete versions of the Gabor transform [83] are popular in signal, speech and image processing.

8.4 Wavelet Analysis

The STFT method uses constant frequency and time resolution. Therefore the lowest frequency of interest determines the minimum width of the window whereas at higher frequencies shorter time windows could be more appropriate to increase time resolution while keeping the relative uncertainty in frequency constant (Fig. 8.12). This is the basic idea of the wavelet transform. Whereas STFT uses wave packets of the form (8.21)

$$\Omega_{t_0,\omega}(t) = W(t - t_0)\mathrm{e}^{\mathrm{i}\omega(t-t_0)} \tag{8.56}$$

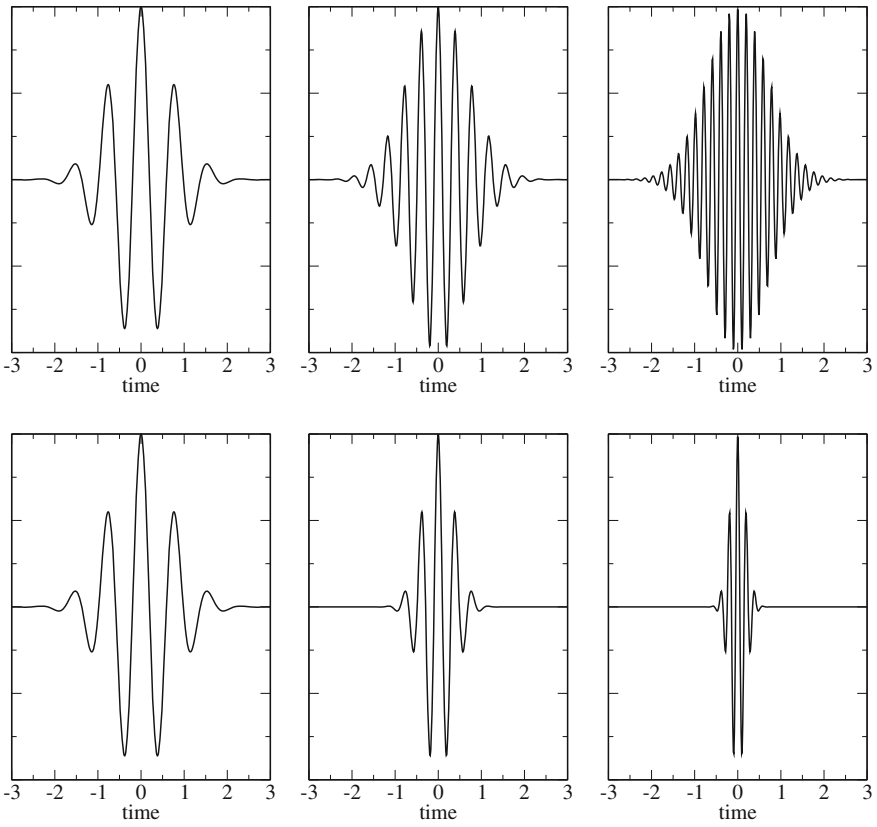

Fig. 8.12 (Morlet wavelets and STFT wave packets) ***Top*** STFT uses the same window for all frequencies ***Bottom*** wavelets use a variable window width to keep the form of the wave packet and the relative frequency resolution constant (only the real part is shown)

where only the oscillating part is scaled with frequency ω, wavelets scale the whole function like in

$$\Omega_{t_0,s}(t) = W\left(\frac{t-t_0}{s}\right) \mathrm{e}^{\mathrm{i}\omega_0(t-t_0)/s} \tag{8.57}$$

or, more generally

$$\Omega_{t_0,s}(t) = \frac{1}{\sqrt{|s|}}\Psi\left(\frac{t-t_0}{s}\right) \tag{8.58}$$

$$\begin{aligned}\tilde{\Omega}(\omega) &= \frac{1}{\sqrt{2\pi}}\int_{-\infty}^{\infty} \mathrm{e}^{-\mathrm{i}\omega t}\frac{1}{\sqrt{|s|}}\Psi\left(\frac{t-t_0}{s}\right)dt \\ &= \frac{1}{\sqrt{2\pi}}\int_{-\infty \mathrm{sign}\, s}^{\infty \mathrm{sign}\, s} \mathrm{e}^{-\mathrm{i}\omega(st'+t_0)}\frac{1}{\sqrt{|s|}}\Psi(t')d(st'+t_0) \\ &= \sqrt{|s|}\mathrm{e}^{-\mathrm{i}\omega t_0}\frac{1}{\sqrt{2\pi}}\int_{-\infty}^{\infty}\mathrm{e}^{-\mathrm{i}\omega s t'}\Psi(t')dt' = \sqrt{|s|}\mathrm{e}^{-\mathrm{i}\omega t_0}\tilde{\Psi}(s\omega)\end{aligned} \tag{8.59}$$

where a whole family of wavelets is derived from the "mother wavelet" $\Psi(t)$ by shifting and rescaling. The prefactor has been introduced to keep the norm invariant

$$\begin{aligned}&\int |\Omega_{t_0,s}(t)|^2 dt = \frac{1}{|s|}\int |\Psi\left(\frac{t-t_0}{s}\right)|^2 dt \\ &= \frac{1}{|s|}\int_{-\infty \mathrm{sign}\, s}^{\infty \mathrm{sign}\, s} |\Psi(t')|^2 d(st'+t_0) = \int |\Psi(t')|^2 dt'.\end{aligned} \tag{8.60}$$

Closely related to the short time Fourier analysis is the Morlet (or Gabor) wavelet, which is also very useful in quantum physics [84]. It is defined as[7]

$$\Psi(t) = W_G(t)\mathrm{e}^{\mathrm{i}\omega_0 t} = \frac{1}{\pi^{1/4}\sqrt{d}}\exp\left\{-\frac{t^2}{2d^2}\right\}\mathrm{e}^{\mathrm{i}\omega_0 t} \tag{8.61}$$

$$\tilde{\Psi}(\omega) = \tilde{W}_G(\omega-\omega_0) = \frac{\sqrt{d}}{\pi^{1/4}}\exp\left\{-\frac{d^2}{2}(\omega-\omega_0)^2\right\}. \tag{8.62}$$

The similarity of a signal $f(t)$ to a wavelet with scale s centered at t_0 is measured by the correlation integral

$$C(t_0,s) = \int_{-\infty}^{\infty} f(t)\Omega^*_{t_0,s}(t)dt = \frac{1}{\sqrt{|s|}}\int_{-\infty}^{\infty}\Psi^*\left(\frac{t-t_0}{s}\right)f(t)dt \tag{8.63}$$

[7] The conventional normalization is $\int dt|\Psi(t)|^2 = 1$.

which becomes a product after Fourier transformation with respect to t_0

$$\begin{aligned}
\tilde{C}(\omega, s) &= \frac{1}{\sqrt{2\pi}} \int C(t_0, s) \mathrm{e}^{-\mathrm{i}\omega t_0} dt_0 \\
&= \frac{1}{\sqrt{2\pi}} \int dt_0 \mathrm{e}^{-\mathrm{i}\omega t_0} \int dt \frac{1}{2\pi} \int d\omega' \sqrt{|s|} \tilde{\Psi}^*(s\omega') \mathrm{e}^{-\mathrm{i}\omega'(t-t_0)} \int d\omega'' \tilde{f}(\omega'') \mathrm{e}^{\mathrm{i}\omega'' t} \\
&= \sqrt{2\pi|s|} \int dt \int d\omega' \tilde{\Psi}^*(s\omega') \mathrm{e}^{-\mathrm{i}\omega' t} \int d\omega'' \tilde{f}(\omega'') \mathrm{e}^{\mathrm{i}\omega'' t} \delta(\omega - \omega') \delta(\omega' - \omega'') \\
&= \sqrt{2\pi|s|} \int d\omega' \tilde{\Psi}^*(s\omega') \mathrm{e}^{-\mathrm{i}\omega' t} \tilde{f}(\omega') \mathrm{e}^{\mathrm{i}\omega' t} \\
&= \sqrt{2\pi|s|} \tilde{\Psi}^*(s\omega) \tilde{f}(\omega). \qquad (8.64)
\end{aligned}$$

For the Morlet wavelet this becomes

$$\begin{aligned}
\tilde{C}(\omega, s) &= \pi^{1/4} \sqrt{2|s|d} \exp\left\{ -\frac{d^2}{2} (s\omega - \omega_0)^2 \right\} \tilde{f}(\omega) \\
&= \pi^{1/4} \sqrt{2|s|d} \exp\left\{ -\frac{(sd)^2}{2} \left(\omega - \frac{\omega_0}{s} \right)^2 \right\} \tilde{f}(\omega) \qquad (8.65)
\end{aligned}$$

i.e. $\tilde{C}(\omega, s)$ averages the spectrum $\tilde{f}$ over a range with a width of $\sigma_\omega = 1/sd$ around $\omega = \omega_0/s$ and a constant ratio

$$\frac{\sigma_\omega}{\omega} = \frac{1}{\omega_0 d}. \qquad (8.66)$$

8.5 Wavelet Synthesis

For data processing it is necessary to reconstruct the data from the wavelet coefficients $C(t_0 s)$. This can be achieved with the help of the integral[8]

$$\begin{aligned}
&\int_{-\infty}^{\infty} \int_{-\infty}^{\infty} \frac{1}{s^2} C(t_0, s) \Omega_{t_0,s}(t) dt_0 ds = \int \frac{1}{s^2} dt_0 ds \frac{1}{\sqrt{|s|}} \Psi\left(\frac{t - t_0}{s} \right) C(t_0, s) \\
&= \frac{1}{\sqrt{2\pi}} \int \frac{1}{s^2} ds \int dt_0 \int d\omega \mathrm{e}^{\mathrm{i}\omega(t-t_0)/s} \tilde{\Psi}(\omega) \int d\omega' \mathrm{e}^{\mathrm{i}\omega' t_0} \tilde{\Psi}^*(s\omega) \tilde{f}(\omega) \\
&= \frac{1}{\sqrt{2\pi}} \int \frac{1}{s^2} ds \int dt_0 \int s d\omega'' \mathrm{e}^{\mathrm{i}\omega''(t-t_0)} \tilde{\Psi}(\omega'' s) \int d\omega' \mathrm{e}^{\mathrm{i}\omega' t_0} \tilde{\Psi}^*(s\omega') \tilde{f}(\omega') \\
&= \frac{1}{\sqrt{2\pi}} \int \frac{1}{s} ds \int d\omega'' \mathrm{e}^{\mathrm{i}\omega'' t} \tilde{\Psi}(\omega'' s) \int d\omega' \tilde{\Psi}^*(s\omega') \tilde{f}(\omega') 2\pi \delta(\omega' - \omega'') \\
&= \sqrt{2\pi} \int \frac{1}{s} ds \int s d\omega'' \mathrm{e}^{\mathrm{i}\omega'' t} \tilde{\Psi}(\omega'' s) \Psi(s\omega'') \tilde{f}(\omega'') \\
&= \sqrt{2\pi} \int \frac{1}{s} ds \int d\omega'' \mathrm{e}^{\mathrm{i}\omega'' t} \tilde{\Psi}(\omega'' s) \tilde{\Psi}^*(s\omega'') \tilde{f}(\omega''). \qquad (8.67)
\end{aligned}$$

[8] A more rigorous treatment introducing the concept of frames in Hilbert space can be found in [85].

If the admissibility condition is fulfilled, which states that the integral

$$C_\Psi = \int_{-\infty}^{\infty} \frac{|\tilde{\Psi}(\omega)|^2}{\omega} d\omega < \infty \tag{8.68}$$

exists and is final, then

$$\int_{-\infty}^{\infty} \frac{1}{s} ds \tilde{\Psi}(\omega s)\tilde{\Psi}^*(\omega s) = \int_{-\infty}^{\infty} \frac{1}{\omega'} d\omega' \tilde{\Psi}(\omega')\tilde{\Psi}^*(\omega') = C_\Psi$$

and we obtain

$$f(t) = \frac{1}{2\pi C_\Psi} \int_{-\infty}^{\infty} \int_{-\infty}^{\infty} \frac{1}{s^2} C(t_0, s) \Omega_{t_0,s}(t) dt_0 ds.$$

The admissibility condition implies that $\tilde{\Psi}(0) = 0$ and thus $\int dt \Psi(t) = 0$. Hence, the Morlet wavelet (8.61) has to be modified[9]

$$\Psi(t) = \frac{1}{\pi^{1/4}\sqrt{d}} N_d \exp\left\{-\frac{t^2}{2d^2}\right\} \left[e^{i\omega_0 t} - \exp\left\{-\frac{\omega_0^2 d^2}{2}\right\}\right] \tag{8.69}$$

$$\tilde{\Psi}(\omega) = \frac{\sqrt{d}}{\pi^{1/4}} N_d \left[\exp\left\{-\frac{d^2}{2}(\omega - \omega_0)^2\right\} - \exp\left\{-\frac{d^2}{2}(\omega^2 + \omega_0^2)\right\}\right] \tag{8.70}$$

$$N_d = \left[\left(1 + \exp\left\{-\omega^2 d^2\right\} - 2\exp\left\{-\frac{3}{4}\omega^2 d^2\right\}\right)\right]^{-1/2}. \tag{8.71}$$

Another popular (continuous) wavelet is the "Mexican hat" (also known as Ricker wavelet or Marr wavelet) which is given by the normalized negative second derivative of a Gaussian (Fig. 8.13)

$$\Psi(t) = \frac{2}{\pi^{1/4}\sqrt{3d}} \left(1 - \frac{t^2}{d^2}\right) \exp\left\{-\frac{t^2}{2d^2}\right\} \tag{8.72}$$

$$\tilde{\Psi}(\omega) = \frac{2\sqrt{d}}{\pi^{1/4}\sqrt{3}} \omega^2 \exp\left\{-\frac{\omega^2 d^2}{2}\right\}. \tag{8.73}$$

Example: Wavelet Analysis of a Nonstationary Signal

The following example shows screen shots from Problem 8.2. The signal consists of two sweeps with linearly increasing frequency of the form

$$f_{1,2}(t) = \sin\left[\omega_{1,2} t + \frac{\alpha_{1,2}}{2} t^2\right] \tag{8.74}$$

[9] This correction is often neglected, if the width is large.

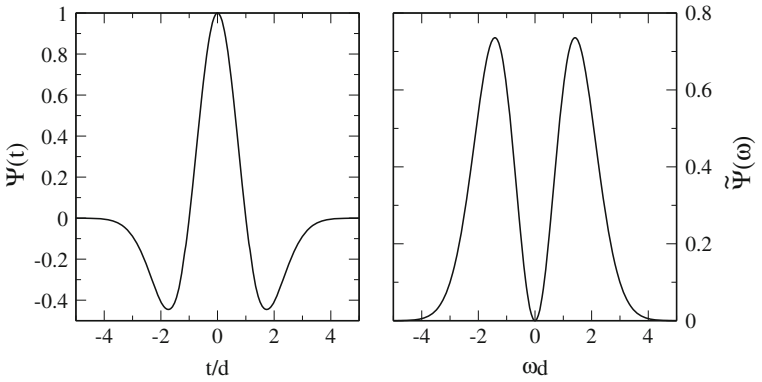

Fig. 8.13 (Mexican hat wavelet) ***Left*** The mexican hat wavelet is essentially the second derivative of a Gaussian. ***Right*** Its Fourier transform is a band pass filter around $\omega_{max} = \pm 2/d$

and another component which switches between a 5 kHz oscillation and the sum of a 300 Hz and a 20 kHz oscillation at a rate of 20 Hz

$$f_3(t) = \begin{cases} \sin(\omega_{20kHz}t) + \sin(\omega_{300Hz}t) & \text{if } \sin(\omega_{20Hz}t) < 0 \\ \sin(\omega_{5kHz}t) & else. \end{cases} \tag{8.75}$$

The signal is sampled with a rate of 44 kHz and analyzed with Morlet wavelets over 6 octaves (Fig. 8.14). The parameter d of the mother wavelet (8.61) determines frequency and time resolution. The frequency ω_0 of the mother wavelet is taken as the Nyquist frequency which is half the sampling rate. The convolution with the daughter wavelets

$$\Psi_{m,n}(t) = \frac{1}{\sqrt{s_m}} \Psi\left(\frac{t - t_n}{s_m}\right) \tag{8.76}$$

is calculated at 400 times with a step size of 0.726 ms (corresponding to 32 samples)

$$t_n = t_0 + n\Delta t \tag{8.77}$$

and for 300 different values of the scaling parameter

$$s_m = 1.015^m. \tag{8.78}$$

In a logarithmic plot, the relative frequency uncertainty has the same size for all stationary signals.

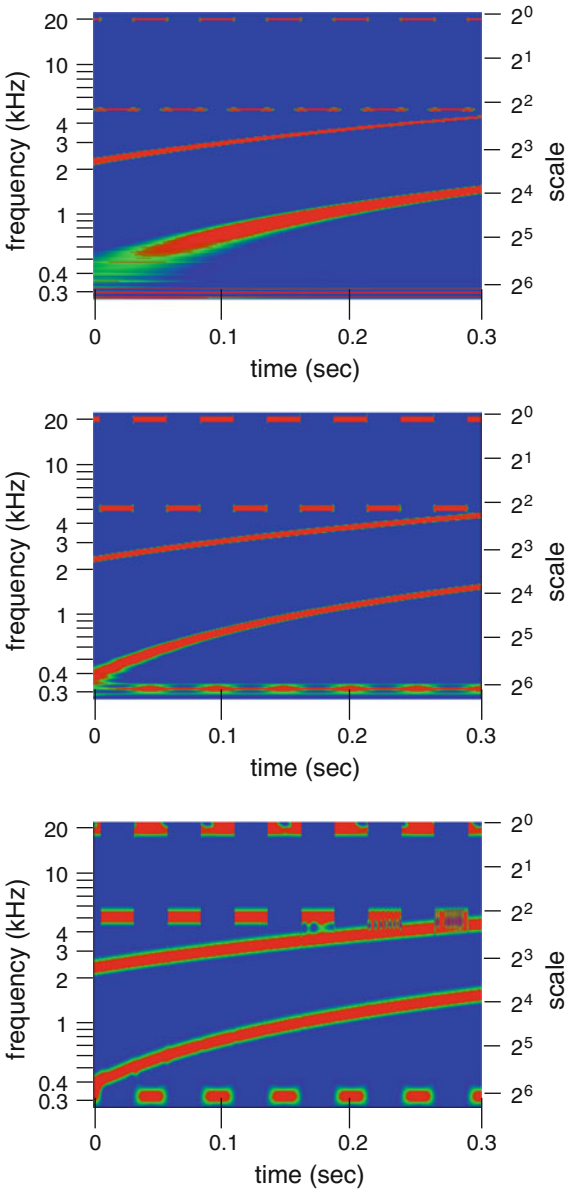

Fig. 8.14 (Wavelet analysis) ***Top*** for $d = 1$ ms the frequency resolution is high for the stationary parts of the signal. Time resolution is low. ***Middle*** for $d = 0.25$ ms the pulsating component at 300 Hz can be resolved but time resolution is still poor. ***Bottom*** For $d = 0.0625$ ms time resolution is sufficient to show all the modulations while frequency resolution is rather poor

8.6 Discrete Wavelet Transform and Multiresolution Analysis

The continuous wavelet transform is very redundant and time consuming. Multiresolution analysis provides a way to define a discrete set of orthogonal wavelets, for which the wavelet transform can be calculated very efficiently from a scalar product. A discrete wavelet transform uses discrete values of shift and scaling parameters

$$s = a^{-m} \quad t_0 = na^{-m}b \tag{8.79}$$

to define the daughter wavelets[10]

$$\Psi_{m,n}(t) = a^{m/2}\Psi\left(a^m t - nb\right). \tag{8.80}$$

For integer a, in most cases $a = 2$, this equation defines wavelets of a multiresolution analysis (Fig. 8.15) where m corresponds to the resolution 2^m.

8.6.1 Scaling Function and Multiresolution Approximation

At the basic resolution 2^0 the function $f(t)$ is approximated as a linear combination

$$f(t) \approx f(t)^{(0)} = \sum_n f_{0,n}\Phi_{0,n}(t) \tag{8.81}$$

of a scaling function and its translations,

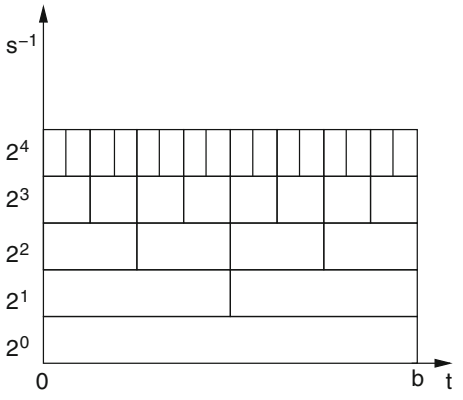

Fig. 8.15 (Multiresolution analysis) Data are analyzed with decreasing time window $\Delta t = b/2^m$

[10] Equation 8.76, in contrast, describes the continuous wavelet transform, which has to be discretized for numerical calculations.

$$\Phi_{0,n} = \Phi(t - nb) \quad , n = 0, \pm 1 \ldots \tag{8.82}$$

which is chosen [86, 87] such, that the $\Phi_{0,n}$ form an orthonormal basis of the space of linear combinations

$$V_0 = \text{span}\{\Phi_{0,n}, n = 0, \pm 1, \ldots\} \tag{8.83}$$

$$\int \Phi^*_{0,n}(t)\Phi_{0,n'}(t)dt = \delta_{n,n'}. \tag{8.84}$$

The best approximation is found by minimizing the norm

$$\begin{aligned} ||f(t) - \sum_n f_{0,n}\Phi_{0n}(t)||^2 &= \int (f^*(t) - \sum_n f^*_{0,n}\Phi^*_{0n}(t))(f(t) - \sum_{n'} f_{0,n'}\Phi_{0n'}(t))dt \\ &= \int |f(t)|^2 dt - \sum_{n'} f_{0n'} \int f^*(t)\Phi_{0n'}(t)dt - \sum_n f^*_{0n}(t) \int \Phi^*_{0n}(t) f(t)dt + \sum_n |f_{0n}|^2 \end{aligned} \tag{8.85}$$

hence by choosing

$$f_{0n} = \int \Phi^*_{0n}(t) f(t)dt \tag{8.86}$$

i.e., the orthogonal projection of $f(t)$ onto V_0. Approximation at the higher resolution 2^m similarly is given by linear combination

$$f(t) \approx f(t)^{(m)} = \sum_n f_{m,n}\Phi_{m,n}(t) \tag{8.87}$$

of the scaled functions

$$\Phi_{m,n} = 2^{m/2}\Phi(2^m t - nb) \tag{8.88}$$

which form an orthonormal basis for the space

$$V_m = \text{span}\{\Phi_{m,n}, n = 0, \pm 1, \ldots\} \tag{8.89}$$

since

$$\begin{aligned} &\int \Phi^*_{m,n}(t)\Phi_{m,n'}(t)dt = 2^m \int \Phi^*(2^m t - nb)\Phi(2^m t - n'b)dt \\ &= 2^m \int \Phi^*(t' - nb)\Phi(t' - n'b)\frac{dt'}{2^m} = \delta_{n,n'}. \end{aligned} \tag{8.90}$$

The sequence of spaces V_m is called a multiresolution approximation to the space of square integrable functions $L^2(\mathbb{R})$, if [86]

$$\text{(i)} \quad \cdots \subset V_{-1} \subset V_0 \subset V_1 \subset V_2 \ldots \tag{8.91}$$

$$\text{(ii)} \quad \bigcup_{m=-\infty}^{\infty} V_m \quad \text{is dense in } L^2(\mathbb{R}) \tag{8.92}$$

$$\text{(iii)} \quad \bigcap_{m=-\infty}^{\infty} V_m = \{0\}. \tag{8.93}$$

Property (ii) has as a consequence, that the approximations $f^{(m)}(t)$ converge to $f(t)$ for large m. Hence, due to orthonormality

$$f^{(m)}(t) = \sum_n \Phi_{m,n}(t) \int_{-\infty}^{\infty} \Phi^*_{m,n}(t') f(t') dt' \to f(t) \tag{8.94}$$

and the projection operator onto V_m

$$P_m = \sum_n \Phi_{m,n}(t) \Phi^*_{m,n}(t') = 2^m \sum_n \Phi(2^m t - nb) \Phi^*(2^m t' - nb) \to 1 \tag{8.95}$$

converges to the unit operator. Now, with $a > 0$ choose the function

$$f_a(t) = \begin{cases} 1 \text{ if } -a \le x \le a \\ 0 \text{ else.} \end{cases} \tag{8.96}$$

Then,

$$\begin{aligned} (P_m f_{ab})(t) &= \sum_n \Phi(2^m t - nb) \int_{-a}^{a} 2^m dt' \Phi^*(2^m t' - nb) \\ &= \sum_n \Phi(2^m t - nb) \int_{-2^m a}^{2^m a} \Phi^*(t' - nb) dt'. \end{aligned} \tag{8.97}$$

For large a, the integrals become more and more independent on n, and

$$\left(\int_{-\infty}^{\infty} \Phi^*(t') dt' \right) \sum_n \Phi(2^m t - nb) \to 1. \tag{8.98}$$

Now we integrate the sum over one period $0 \le t \le 2^{-m} b$ and find

$$\int_0^{2^{-m} b} \sum_n \Phi(2^m t - nb) dt = \sum_n \int_{-nb}^{(1-n)b} \Phi(t)\, 2^{-m} dt = 2^{-m} \int_{-\infty}^{\infty} \Phi(t) dt \tag{8.99}$$

and therefore

$$\left(\int_{-\infty}^{\infty} \Phi^*(t')dt'\right)\left(\int_{-\infty}^{\infty} \Phi(t')dt'\right) = b \tag{8.100}$$

or

$$\left|\int_{-\infty}^{\infty} \Phi(t')dt'\right| = \sqrt{b} \tag{8.101}$$

as well as

$$|\tilde{\Phi}(0)| = \frac{1}{\sqrt{2\pi}}\left|\int_{-\infty}^{\infty} \Phi(t')dt'\right| = \sqrt{\frac{b}{2\pi}}. \tag{8.102}$$

Fourier transformation of (8.84) gives

$$\begin{aligned}
\delta_{nn'} &= \int \Phi^*(t-nb)\Phi(t-n'b)dt \\
&= \frac{1}{2\pi}\int dt \int \tilde{\Phi}^*(\omega)\mathrm{e}^{-\mathrm{i}\omega(t-nb)}d\omega \int \tilde{\Phi}(\omega')\mathrm{e}^{\mathrm{i}\omega'(t-n'b)}d\omega' \\
&= \int d\omega d\omega' \tilde{\Phi}^*(\omega)\tilde{\Phi}(\omega')\mathrm{e}^{\mathrm{i}(\omega n-\omega' n')b}\delta(\omega-\omega') = \int d\omega |\tilde{\Phi}(\omega)|^2 \mathrm{e}^{\mathrm{i}\omega(n-n')b} \\
&= \sum_{j=-\infty}^{\infty}\int_{2\pi j/b}^{2\pi(j+1)/b} d\omega |\tilde{\Phi}(\omega)|^2 \mathrm{e}^{\mathrm{i}\omega(n-n')b} = \int_0^{2\pi/b} d\omega \sum_{j=-\infty}^{\infty} |\tilde{\Phi}(\omega+2\pi j/b)|^2 \mathrm{e}^{-\mathrm{i}\omega\Delta nb} \\
&= \int_0^{2\pi/b} d\omega F(\omega)\mathrm{e}^{-\mathrm{i}\omega\Delta nb}.
\end{aligned} \tag{8.103}$$

$F(\omega)$ is periodic with period $\Omega_0 = 2\pi/b$ and can be represented as a Fourier sum

$$F(\omega) = \sum_{n=-\infty}^{\infty} F_n \mathrm{e}^{\mathrm{i}2\pi n\omega/\Omega_0} = \sum_{n=-\infty}^{\infty} F_n \mathrm{e}^{\mathrm{i}nb\omega} \tag{8.104}$$

where the Fourier coefficients

$$F_n = \frac{1}{\Omega_0}\int_0^{\Omega_0} F(\omega)\mathrm{e}^{-\mathrm{i}2\pi n\omega/\Omega_0} = \frac{b}{2\pi}\int_0^{2\pi/b} F(\omega)\mathrm{e}^{-\mathrm{i}nb\omega} \tag{8.105}$$

are found from comparison with (8.103)

$$F_n = \frac{b}{2\pi}\delta_{n,0}. \tag{8.106}$$

Finally, evaluation of the Fourier sum (8.104) gives

$$F(\omega) = \sum_j |\tilde{\Phi}(\omega + j\Omega_0)|^2 = \frac{1}{\Omega_0} \tag{8.107}$$

which is the equivalent of the orthonormality of Φ_{0n} in Fourier space.

Equation 8.91 implies that $\Phi_{m,n}$ can be represented as linear combination of the $\Phi_{m+1,n}$. Starting from

$$\Phi(t) = \Phi_{0,0}(t) = \sum_n h_n \Phi_{1,n}(t) = \sqrt{2} \sum_n h_n \Phi(2t - nb) \tag{8.108}$$

scaling and translation gives

$$\Phi_{m,n}(t) = \sum_{n'} h_{n'-2n} \Phi_{m+1,n'}(t). \tag{8.109}$$

Fourier transformation of (8.88) gives

$$\tilde{\Phi}_{m,n}(\omega) = \mathrm{e}^{-2n\pi \mathrm{i}\omega/\Omega_m} \tilde{\Phi}_{m,0}(\omega) = \frac{1}{\sqrt{2^m}} \mathrm{e}^{-2n\pi \mathrm{i}\omega/\Omega_m} \tilde{\Phi}(\omega/2^m) \tag{8.110}$$

$$\tilde{\Phi}_{m+1,n}(\omega) = \frac{1}{\sqrt{2}} \tilde{\Phi}_{mn}(\omega/2) \tag{8.111}$$

with

$$\Omega_m = 2^m \frac{2\pi}{b} = 2^m \Omega_0 \tag{8.112}$$

and (8.108) becomes

$$\tilde{\Phi}(\omega) = \sum_n \frac{h_n}{\sqrt{2}} \mathrm{e}^{-2n\pi \mathrm{i}\omega/\Omega_1} \tilde{\Phi}(\omega/2^m) = M_0(\omega/2) \tilde{\Phi}(\omega/2) \tag{8.113}$$

where

$$M_0(\omega/2) = \sum_n \frac{h_n}{\sqrt{2}} \mathrm{e}^{-2n\pi \mathrm{i}(\omega/2)/\Omega_0} \tag{8.114}$$

is Ω_0-periodic. Similarly, we find

$$\tilde{\Phi}_{m0}(\omega) = \sum_n h_n \tilde{\Phi}_{m+1n}(\omega) = \sum_n \frac{h_n}{\sqrt{2^{m+1}}} \mathrm{e}^{-2n\pi \mathrm{i}(\omega/2^{m+1})/\Omega_0} \tilde{\Phi}(\omega/2^{m+1})$$
$$= \frac{1}{\sqrt{2^m}} M_0(\omega/2^{m+1}) \tilde{\Phi}(\omega/2^{m+1}). \tag{8.115}$$

Equation 8.113 can be iterated to obtain

$$\tilde{\Phi}(\omega) = M_0(\omega/2)\tilde{\Phi}(\omega/2) = M_0(\omega/2)M_0(\omega/4)\tilde{\Phi}(\omega/4) = \ldots$$
$$= \prod_{j=1}^{\infty} M_0(\omega/2^j)\tilde{\Phi}(0) = \prod_{j=1}^{\infty} M_0(\omega/2^j)\sqrt{\frac{b}{2\pi}}. \tag{8.116}$$

This equation shows that knowledge of M_0 is sufficient to determine the scaling function (see also p. 182).

From the orthogonality condition (8.107) we obtain

$$\frac{1}{\Omega_0} = \sum_j |\tilde{\Phi}(\omega + j\Omega_0)|^2 = \sum_j \left| M_0\left(\omega/2 + j\frac{\Omega}{2}\right)\right|^2 \left|\tilde{\Phi}\left(\omega/2 + j\frac{\Omega}{2}\right)\right|^2$$
$$= \sum_j |M_0(\omega/2 + j\Omega_0)|^2 |\tilde{\Phi}(\omega/2 + j\Omega_0)|^2$$
$$+ \sum_j \left| M_0\left(\omega/2 + \left(j + \frac{1}{2}\right)\Omega_0\right)\right|^2 \left|\tilde{\Phi}\left(\omega/2 + \left(j + \frac{1}{2}\right)\Omega_0\right)\right|^2$$
$$= |M_0(\omega/2)|^2 \sum_j |\tilde{\Phi}(\omega/2 + j\Omega_0)|^2$$
$$+ \left| M_0\left(\omega/2 + \frac{\Omega_0}{2}\right)\right|^2 \sum_j |\tilde{\Phi}((\omega + \Omega_0)/2 + j\Omega_0)|^2$$
$$= \frac{1}{\Omega_0}\left[|M_0(\omega/2)|^2 + \left|M_0\left(\omega/2 + \frac{\Omega_0}{2}\right)\right|^2\right]. \tag{8.117}$$

Example: Rectangular Scaling Function

The simplest example of a scaling function is the rectangular function

$$\Phi(t) = \begin{cases} \frac{1}{\sqrt{b}} & \text{for } \left|t - \frac{b}{2}\right| \leq \frac{b}{2} \\ 0 & \text{else} \end{cases} \tag{8.118}$$

with the scaled and translated functions

$$\Phi_{0,n}(t) = \Phi(t - nb) = \begin{cases} \frac{1}{\sqrt{b}} & \text{for } \left|t - \left(n + \frac{1}{2}\right) b\right| \le \frac{b}{2} \\ 0 & \text{else} \end{cases} \tag{8.119}$$

$$\Phi_{1,n}(t) = \sqrt{2}\Phi(2t - nb) = \begin{cases} \frac{1}{\sqrt{b/2}} & \text{for } \left|t - \left(n + \frac{1}{2}\right) \frac{b}{2}\right| \le \frac{b}{4} \\ 0 & \text{else} \end{cases} \tag{8.120}$$

$$\vdots$$

$$\Phi_{m,n}(t) = \sqrt{2^m}\Phi(2^m t - nb) = \begin{cases} \frac{1}{\sqrt{b/2^m}} & \text{for } \left|t - \left(n + \frac{1}{2}\right) \frac{b}{2^m}\right| < \frac{b}{2^{m+1}} \\ 0 & \text{else} \end{cases}. \tag{8.121}$$

Obviously, the $\Phi_{mn}(t)$ for fixed m are orthonormal and can be represented as linear combination

$$\Phi_{m,n}(t) = \frac{1}{\sqrt{2}}\Phi_{m+1,2n}(t) + \frac{1}{\sqrt{2}}\Phi_{m+1,2n+1}(t). \tag{8.122}$$

V_m is the space of functions which are piecewise constant on intervals $|t - (n + 1/2)b/2^m| < b/2^{m+1}$. Figure 8.16 shows the approximation of the parabola $f(t) = t^2$ by functions in $V_0 \ldots V_3$.

The Fourier transform of the scaling function is

$$\tilde{\Phi}(\omega) = \frac{1}{\sqrt{2\pi}} \frac{2\sin\left(\frac{\omega b}{2}\right)}{\omega\sqrt{b}} \mathrm{e}^{-\mathrm{i}\omega b/2} = \frac{\sqrt{b}}{\sqrt{2\pi}} \mathrm{sinc}\left(\frac{\omega b}{2}\right) \mathrm{e}^{-\mathrm{i}\omega b/2} \tag{8.123}$$

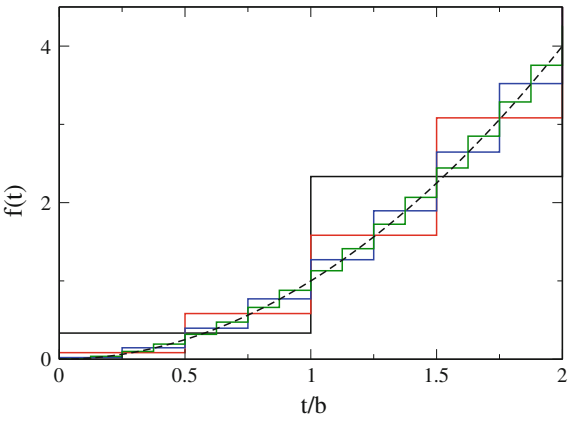

Fig. 8.16 (Approximation by piecewise constant functions) The parabola $f(t) = t^2$ (*dashed curve*) is approximated by linear combination of orthonormal rectangular functions (8.121) $f_m(t) = \sum_n \Phi_{mn}(t) \int_{-\infty}^{\infty} \Phi_{mn}^*(t) f(t) dt$ for $m = 0$ (*black*) $m = 1$ (*red*) $m = 2$ (*blue*) $m = 3$ (*green*)

and from

$$\tilde{\Phi}(\omega) = \frac{1}{\sqrt{2\pi}} \frac{2\left[2\sin\left(\frac{\omega b}{4}\right)\cos\left(\frac{\omega b}{4}\right)\right]}{\omega\sqrt{b}} \mathrm{e}^{-\mathrm{i}\omega b/2} = \tilde{\Phi}\left(\frac{\omega b}{2}\right)\cos\left(\frac{\omega b}{4}\right)\mathrm{e}^{-\mathrm{i}\omega b/4} \tag{8.124}$$

we find

$$M_0\left(\frac{\omega}{2}\right) = \cos\left(\frac{\omega b}{4}\right)\mathrm{e}^{-\mathrm{i}\omega b/4}. \tag{8.125}$$

8.6.2 Construction of an Orthonormal Wavelet Basis

The approximation $f^{(m+1)}(t)$ contains more details than $f^{(m)}(t)$. We would like to extract these details by dividing the space

$$V_{m+1} = V_m + W_m \tag{8.126}$$

into the sum of V_m and an orthogonal complement $W_m \perp V_m$. The approximation $f^{(m+1)}(t)$ then can be divide into the approximation $f^{(m)}$ plus the projection onto W_m, which provides the details. In the following we will construct an orthonormal basis of W_m in terms of wavelet functions $\Psi(t)$ which have the properties

$$\text{(i)} \quad \Psi \in V_{m+1} \tag{8.127}$$

or

$$\Psi = \sum_n C_n \Phi_{m+1,n} \tag{8.128}$$

and

$$\text{(ii)} \quad \Psi \perp V_m \tag{8.129}$$

or

$$\int_{-\infty}^{\infty} \Psi^*(t)\Phi_{mn}(t)dt = 0 \quad \forall n \tag{8.130}$$

which is equivalent to

$$\int_{-\infty}^{\infty} \tilde{\Psi}^*(\omega)\tilde{\Phi}_{mn}(\omega)d\omega = 0 \quad \forall n. \tag{8.131}$$

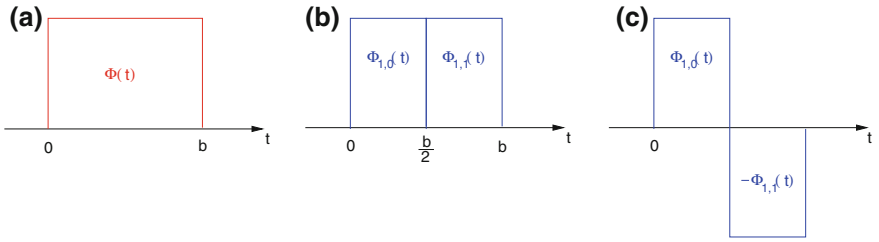

Fig. 8.17 (Haar wavelet) The rectangular scaling function (**a**) can be written as a linear combination of translated scaling functions at the next higher resolution (**b**). This is also the case for the wavelet function (**c**) which is orthogonal to the scaling function

Example: Haar Wavelet

With the rectangular scaling function

$$\Phi(t) = \begin{cases} 1 \text{ if } 0 \le x \le 1 \\ 0 \text{ else} \end{cases} \tag{8.132}$$

the Haar wavelet [88] (Fig. 8.17)

$$\Psi(t) = \frac{1}{\sqrt{2}}\Phi_{1,0}(t) - \frac{1}{\sqrt{2}}\Phi_{1,0}(t) \tag{8.133}$$

is a linear combination of the translated functions $\Phi_{1,n}$ and orthogonal to all $\Phi_{0,n}$. The family of scaled and translated daughter wavelets

$$\Psi_{m,n}(t) = \frac{1}{\sqrt{2}}\Phi_{m,n}(t) - \frac{1}{\sqrt{2}}\Phi_{m,n+1}(t)$$

obeys

$$\Psi_{m,n} \in V_{m+1} \quad \Psi_{m,n} \perp V_m. \tag{8.134}$$

Orthogonality Condition

After Fourier transformation, (8.131) becomes

$$\begin{aligned} 0 &= \int \tilde{\Psi}^*(\omega) \mathrm{e}^{-n\mathrm{i}\omega 2\pi/\Omega_m} \tilde{\Phi}_{m0}(\omega) d\omega \\ &= \sum_j \int_{j\Omega_m}^{(j+1)\Omega_m} \tilde{\Psi}^*(\omega) \mathrm{e}^{-n\mathrm{i}\omega 2\pi/\Omega_m} \tilde{\Phi}_{m0}(\omega) d\omega \end{aligned}$$

$$
\begin{aligned}
&= \sum_j \int_0^{\Omega_m} \tilde{\Psi}^*(\omega + j\Omega_m) \mathrm{e}^{-n\mathrm{i}(\omega + j2\pi/t_m)t_m} \tilde{\Phi}_{m0}(\omega + j\Omega_m) d\omega \\
&= \int_0^{\Omega_m} \mathrm{e}^{-n\mathrm{i}\omega 2\pi/\Omega_m} \sum_j \tilde{\Psi}^*(\omega + j\Omega_m) \tilde{\Phi}_{m0}(\omega + j\Omega_m) d\omega \\
&= \int_0^{\Omega_m} \mathrm{e}^{-n\mathrm{i}\omega 2\pi/\Omega_m} G(\omega) d\omega = \Omega_m \hat{G}(t_n).
\end{aligned} \tag{8.135}
$$

This expression looks like the Fourier coefficient of an Ω_m-periodic function with the Fourier sum (7.5 with ω and t exchanged)

$$
G(\omega) = \sum_{n=-\infty}^{\infty} \mathrm{e}^{\mathrm{i}t_n\omega} \hat{G}(t_n) \text{ with } t_n = n\frac{2\pi}{\Omega_m}. \tag{8.136}
$$

But, since $\hat{G}(t) = 0$, we obtain the orthogonality condition

$$
\sum_j \tilde{\Psi}^*(\omega + j\Omega_m) \tilde{\Phi}_{m0}(\omega + j\Omega_m) = 0. \tag{8.137}
$$

Construction of the Wavelet

Now, Ψ and Φ_{m0} both are in V_{m+1}, therefore (8.113)

$$
\tilde{\Phi}_{m0} = M_{m0}(\omega/2^{m+1}) \tilde{\Phi}(\omega/2^{m+1}) \tag{8.138}
$$

$$
\tilde{\Psi} = M_{\Psi}(\omega/2^{m+1}) \tilde{\Phi}(\omega/2^{m+1}) \tag{8.139}
$$

where $M_{m,0}$ and M_{Ψ} are Ω_0-periodic.

Hence, from (8.137)

$$
\begin{aligned}
0 &= \sum_j M_{\Psi}^*((\omega + j\Omega_m)/2^{m+1}) M_{m0}((\omega + j\Omega_m)/2^{m+1}) |\tilde{\Phi}((\omega + j\Omega_m)/2^{m+1})|^2 \\
&= \sum_j M_{\Psi}^*(\omega/2^{m+1} + j\Omega_0/2) M_{m0}(\omega/2^{m+1} + j\Omega_0/2) |\tilde{\Phi}(\omega/2^{m+1} + j\Omega_0/2)|^2 \\
&= \sum_{j\,even} M_{\Psi}^*(\omega/2^{m+1}) M_{m0}(\omega/2^{m+1}2) |\tilde{\Phi}(\omega/2^{m+1} + \Omega_0 j/2)|^2 \\
&+ \sum_{j\,odd} M_{\Psi}^*\left(\omega/2^{m+1} + \frac{\Omega_0}{2}\right) M_{m0}\left(\omega/2^{m+1} + \frac{\Omega_0}{2}\right) |\tilde{\Phi}(\omega/2^{m+1} + \Omega_0 j/2)|^2 \\
&= M_{\Psi}^*(\omega/2^{m+1}) M_{m0}(\omega/2^{m+1}2) \sum_{j\,even} |\tilde{\Phi}(\omega/2^{m+1} + \Omega_0 j/2)|^2 \\
&+ M_{\Psi}^*\left(\omega/2^{m+1} + \frac{\Omega_0}{2}\right) M_{m0}\left(\omega/2^{m+1} + \frac{\Omega_0}{2}\right) \sum_{j\,odd} |\tilde{\Phi}(\omega/2^{m+1} + \Omega_0 j/2)|^2.
\end{aligned} \tag{8.140}
$$

From orthogonality of $\Phi_{m+1,n}$

$$\sum_j |\tilde{\Phi}(\omega/2^{m+1} + j\Omega_0)|^2 = \frac{1}{\Omega_0} \tag{8.141}$$

we see that both sums have the same value

$$\sum_{j\,even} |\tilde{\Phi}(\omega/2^{m+1} + \Omega_0 j/2)|^2 = \sum_k |\tilde{\Phi}(\omega/2^{m+1} + k\Omega_0)|^2 = \frac{1}{\Omega_0} \tag{8.142}$$

$$\sum_{j\,odd} |\tilde{\Phi}(\omega/2^{m+1} + \Omega_0 j/2)|^2 = \sum_k |\tilde{\Phi}(\omega/2^{m+1} + k\Omega_0 + \Omega_0/2)|^2 = \frac{1}{\Omega_0} \tag{8.143}$$

and therefore

$$M_\Psi^*(\omega/2^{m+1}) M_{m0}(\omega/2^{m+1}2) + M_\Psi^*\left(\omega/2^{m+1} + \frac{\Omega_0}{2}\right) M_{m0}\left(\omega/2^{m+1} + \frac{\Omega_0}{2}\right) = 0 \tag{8.144}$$

which can be satisfied by choosing [86]

$$M_\Psi(\omega/2^{m+1}) = M_{m0}^*\left(\omega/2^{m+1} + \frac{\Omega_0}{2}\right) \mathrm{e}^{\mathrm{i}\omega 2\pi/\Omega_{m+1}} \tag{8.145}$$

which implies

$$\begin{aligned} &M_\Psi\left(\omega/2^{m+1} + \frac{\Omega_0}{2}\right) = M_{m0}^*(\omega/2^{m+1} + \Omega_0)\mathrm{e}^{\mathrm{i}(\omega+\Omega_{m+1}/2)2\pi/\Omega_{m+1}} \\ &= -M_{m0}^*(\omega/2^{m+1})\mathrm{e}^{\mathrm{i}\omega 2\pi/\Omega_{m+1}}. \end{aligned} \tag{8.146}$$

Hence we obtain the solution

$$\begin{aligned} \tilde{\Psi}_m(\omega) &= \mathrm{e}^{\mathrm{i}\omega 2\pi/\Omega_{m+1}} M_{m0}^*\left(\omega/2^{m+1} + \frac{\Omega_0}{2}\right) \tilde{\Phi}(\omega/2^{m+1}) \\ &= \sum_{n'} \frac{h_{n'}^*}{\sqrt{2^{m+1}}} \mathrm{e}^{\mathrm{i}n'\pi} \mathrm{e}^{\mathrm{i}(n'+1)\omega 2\pi/\Omega_{m+1}} \tilde{\Phi}(\omega/2^{m+1}) \end{aligned} \tag{8.147}$$

which becomes in the time domain

$$\Psi_m(t) = \sum_{n'} \frac{h^*_{n'}}{\sqrt{2^{m+1}}}(-1)^{n'} \frac{1}{\sqrt{2\pi}} \int d\omega \mathrm{e}^{\mathrm{i}\omega t} \mathrm{e}^{\mathrm{i}(n'+1)\omega 2\pi/\Omega_{m+1}} \tilde{\Phi}(\omega/2^{m+1})$$

$$= \sum_{n'} (-1)^{n'} h^*_{n'} \sqrt{2^{m+1}} \Phi(2^{m+1}t + (n'+1)b)$$

$$= \sum_{n'} (-1)^{n'} h^*_{n'} \Phi_{m+1,-n'-1}(t) \tag{8.148}$$

$$= \sum_{n} (-1)^{-n-1} h^*_{-n-1} \Phi_{m+1,n}(t). \tag{8.149}$$

From the orthogonality condition (8.107) we obtain

$$\sum_j |\tilde{\Psi}_0(\omega + j\Omega_0)|^2 = \sum \left| M_{00}\left(\omega/2 + (j+1)\frac{\Omega_0}{2}\right)\right|^2 \left|\tilde{\Phi}\left(\omega/2 + j\frac{\Omega_0}{2}\right)\right|^2$$

$$= \sum \left| M_{00}\left(\omega/2 + (2j+1)\frac{\Omega_0}{2}\right)\right|^2 \left|\tilde{\Phi}\left(\omega/2 + 2j\frac{\Omega_0}{2}\right)\right|^2$$

$$+ \sum \left| M_{00}\left(\omega/2 + (2j+2)\frac{\Omega_0}{2}\right)\right|^2 \left|\tilde{\Phi}\left(\omega/2 + (2j+1)\frac{\Omega_0}{2}\right)\right|^2$$

$$= \left| M_{00}\left(\omega/2 + \frac{\Omega_0}{2}\right)\right|^2 \sum |\tilde{\Phi}(\omega/2 + j\Omega_0)|^2$$

$$+ |M_{00}(\omega/2)|^2 \sum |\tilde{\Phi}((\omega + \Omega_0)/2 + j\Omega_0)|^2$$

$$= \frac{1}{\Omega_0}\left(\left| M_{00}\left(\omega/2 + \frac{\Omega_0}{2}\right)\right|^2 + |M_{00}(\omega/2)|^2 \right). \tag{8.150}$$

But, since the scaling function obeys the orthonormality condition (8.107),

$$\frac{1}{\Omega_0} = \sum |\tilde{\Phi}(\omega + j\Omega_0)|^2 = \sum \left| M_{00}\left(\omega/2 + j\frac{\Omega}{2}\right)\right|^2 \left|\tilde{\Phi}\left(\omega/2 + j\frac{\Omega}{2}\right)\right|^2$$

$$= \sum |M_{00}(\omega/2 + j\Omega_0)|^2 |\tilde{\Phi}(\omega/2 + j\Omega_0)|^2$$

$$+ \sum \left| M_{00}\left(\omega/2 + \left(j + \frac{1}{2}\right)\Omega_0\right)\right|^2 \left|\tilde{\Phi}\left(\omega/2 + \left(j + \frac{1}{2}\right)\Omega_0\right)\right|^2$$

$$= |M_{00}(\omega/2)|^2 \sum |\tilde{\Phi}(\omega/2 + j\Omega_0)|^2$$

$$+ \left| M_{00}\left(\omega/2 + \frac{\Omega_0}{2}\right)\right|^2 \sum |\tilde{\Phi}((\omega + \Omega_0)/2 + j\Omega_0)|^2$$

$$= \frac{1}{\Omega_0}\left[|M_{00}(\omega/2)|^2 + \left| M_{00}\left(\omega/2 + \frac{\Omega_0}{2}\right)\right|^2 \right] \tag{8.151}$$

hence the wavelet also fulfills the orthonormality condition

$$\sum_j |\tilde{\Psi}_0(\omega + j\Omega_0)|^2 = \frac{1}{\Omega_0}. \tag{8.152}$$

Therefore the translated wavelet functions

$$\Psi_{mn}(t) = \Psi_m(t - n2^{-m}b) = \sum_{n'} (-1)^{-n'-1} h^*_{-n'-1} \sqrt{2^{m+1}} \Phi(2^{m+1}(t - n2^{-m}b) - n'b)$$
$$= \sum_{n'} (-1)^{-n'-1} h^*_{-n'-1} \Phi_{m+1,2n+n'}(t) \tag{8.153}$$

are orthonormal

$$\int \Psi^*_{mn}(t)\Psi_{mn'}(t)dt = \delta_{n.n'}. \tag{8.154}$$

Wavelets for different resolution m are orthogonal since they are by construction in orthogonal spaces. The $\Psi_{mn}(t)$ with $m, n = -\infty \ldots \infty$ provide an orthonormal basis of

$$L^2(\mathbb{R}) = \bigcup_{m=-\infty}^{\infty} W_m. \tag{8.155}$$

Alternatively, (8.155) is replaced by

$$L^2(\mathbb{R}) = V_0 + \bigcup_{m=0}^{\infty} W_m \tag{8.156}$$

which is more useful for practical applications with limited total observation time. According to (8.156), starting from a basic approximation in V_0, more and more details are added to obtain approximations with increasing accuracy.

Example: Meyer Wavelet

Meyer introduced the first non trivial wavelet (Fig. 8.18) which, in contrast to the Haar wavelet is differentiable [89, 90]. It was originally defined by its scaling function in Fourier space[11] (here, $b = 1$)

$$\tilde{\Phi}(\omega) = \begin{cases} \frac{1}{\sqrt{2\pi}} & \text{if } \omega \le \frac{2\pi}{3} \\ \frac{1}{\sqrt{2\pi}} \cos\left(\frac{\pi}{2}\left(\frac{3|\omega|}{2\pi} - 1\right)\right) & \text{if } \frac{2\pi}{3} < |\omega| < \frac{4\pi}{3} \\ 0 & \text{if } |\omega| > \frac{4\pi}{3} \end{cases} \tag{8.157}$$

from which the mother wavelet can be derived

[11] There are different variants of the Meyer wavelet in the literature.

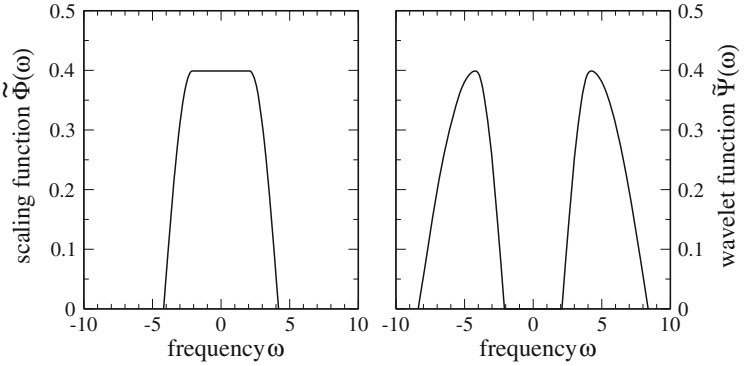

Fig. 8.18 (Meyer wavelet in frequency space) ***Left*** scaling function ***Right*** magnitude of the wavelet function

$$\tilde{\Psi}(\omega) = \begin{cases} \frac{1}{\sqrt{2\pi}} \sin\left(\frac{\pi}{2}\left(\frac{3|\omega|}{2\pi} - 1\right)\right) \mathrm{e}^{\mathrm{i}\omega/2} & \text{if } \frac{2\pi}{3} \leq |\omega| \leq \frac{4\pi}{3} \\ \frac{1}{\sqrt{2\pi}} \cos\left(\frac{\pi}{2}\left(\frac{3|\omega|}{4\pi} - 1\right)\right) \mathrm{e}^{\mathrm{i}\omega/2} & \text{if } \frac{4\pi}{3} \leq |\omega| \leq \frac{8\pi}{3} \\ 0 & \text{else.} \end{cases} \tag{8.158}$$

Explicit expressions in the time domain (Fig. 8.19) were given in 2015 [91]

$$\Phi(t) = \begin{cases} \frac{2}{3} + \frac{4}{3\pi} & \text{if } t = 0 \\ \frac{\sin\frac{2\pi}{3}t + \frac{4}{3}t\cos\frac{4\pi}{3}t}{\pi t - \frac{16\pi}{9}t^3} & \text{else} \end{cases} \tag{8.159}$$

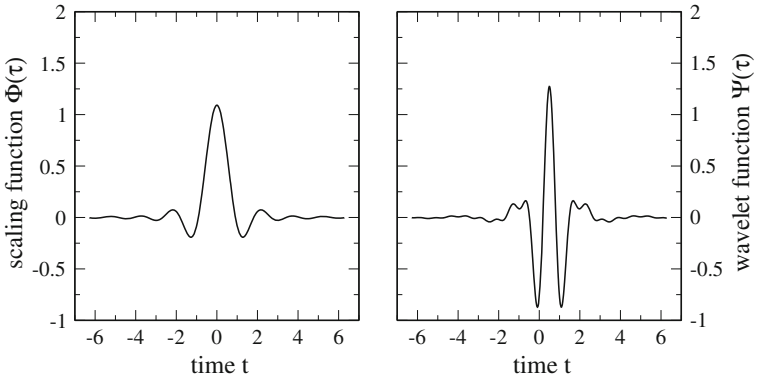

Fig. 8.19 (Meyer wavelet in the time domain) ***Left*** scaling function ***Right*** wavelet function

$$\Psi(t) = \frac{\frac{4}{3\pi}\left(t-\frac{1}{2}\right)\cos\left[\frac{2\pi}{3}\left(t-\frac{1}{2}\right)\right] - \frac{1}{\pi}\sin\left[\frac{4\pi}{3}\left(t-\frac{1}{2}\right)\right]}{\left(t-\frac{1}{2}\right) - \frac{16}{9}\left(t-\frac{1}{2}\right)^3} + \frac{\frac{8}{3\pi}\left(t-\frac{1}{2}\right)\cos\left[\frac{8\pi}{3}\left(t-\frac{1}{2}\right)\right] + \frac{1}{\pi}\sin\left[\frac{4\pi}{3}\left(t-\frac{1}{2}\right)\right]}{\left(t-\frac{1}{2}\right) - \frac{64}{9}\left(t-\frac{1}{2}\right)^3}. \tag{8.160}$$

8.7 Discrete Data and Fast Wavelet Transform

Mallet's algorithm [87] starts with function values

$$f_n = f(n\Delta t_s) \tag{8.161}$$

sampled at multiples of

$$\Delta t_s = 1/f_s = b/2^{m_{max}}. \tag{8.162}$$

We do not really approximate the function but from the series of sample values we construct the linear combination

$$\sum_n f_n \Phi_{m_{max},n}(t) \tag{8.163}$$

which is an element of

$$V_{m_{max}} = V_0 + \bigcup_{m=0}^{m_{max}-1} W_m \tag{8.164}$$

and can therefore be represented as a coarse approximation in V_0 and a series of details with increasing resolution

$$\sum_n f_n \Phi_{m_{max},n}(t) = \sum_n c_n \Phi_{0,n}(t) + \sum_{m=0}^{m_{max}-1} \sum_n d_{mn} \Psi_{mn}(t). \tag{8.165}$$

8.7.1 Recursive Wavelet Transformation

The approximation coefficients c_n and detail coefficients d_{mn} are determined recursively which avoids the calculation of scalar products.

Starting with

$$c_{m_{max},n} = f_n \tag{8.166}$$

the details are extracted by expanding

$$\sum_n c_{m_{max},n}\Phi_{m_{max},n}(t) = \sum_n c_{m_{max}-1,n}\Phi_{m_{max}-1,n}(t) + \sum_n d_{m_{max}-1,n}\Psi_{m_{max}-1,n}(t). \tag{8.167}$$

Due to orthogonality, the coefficients at the next lower resolution can be determined from

$$c_{m_{max}-1,n'} = \sum_n c_{m_{max},n} < \Phi_{m_{max}-1,n'}|\Phi_{m_{max},n} >= \sum_n c_{m_{max},n}h^*_{n-2n'}$$
$$= \sum_n c_{m_{max},n+2n'}h^*_n \tag{8.168}$$

$$d_{m_{max}-1,n'} = \sum_n c_{m_{max},n} < \Psi_{m_{max}-1,n'}|\Phi_{m_{max},n} >= \sum_n c_{m_{max},n}(-1)^{n-1}h_{2n'-n-1} \tag{8.169}$$

which can be written as

$$d_{m_{max}-1,n'} = \sum_n c_{m_{max},n}g^*_{n-2n'} = \sum_n c_{m_{max},n+2n'}g^*_n \quad \text{with } g^*_n = (-1)^{n-1}h_{-n-1}. \tag{8.170}$$

Iterating this recursion allows the calculation of the wavelet coefficients even without explicit knowledge of the scaling and wavelet functions. Equations (8.168) and (8.170) have the form of discrete digital filter functions with subsequent downsampling by a factor of two (dropping samples with odd n').[12] This can be seen by defining the down sampled coefficients

$$c^{\downarrow}_{n'/2} = \sum_n c_n h^*_{n-n'} \tag{8.171}$$

$$d^{\downarrow}_{n'/2} = \sum c_n(-1)^{n-1}h_{n'-n-1} \tag{8.172}$$

and applying the z-transform to (8.168) and (8.170). For the approximation filter we obtain

[12] For the more general class of bi-orthogonal wavelets, a different filter pair is used for reconstruction.

$$f_c(z) = \sum_{n'=-\infty}^{\infty} \sum_{n=-\infty}^{\infty} h_n^* c_{n+n'} z^{-n'}$$

$$= \sum_n h_n^* z^n \sum_{n'} c_{n+n'} z^{-n'-n} = \left(\sum_n h_n z^{-n} \right)^* \sum_{n'} c_{n'} z^{-n'} = h^*(z)\, c(z) \tag{8.173}$$

hence in frequency space the signal is multiplied with the filter function

$$h(\mathrm{e}^{\mathrm{i}\omega\Delta t}) = \sum_n h_n \mathrm{e}^{-n\mathrm{i}\omega\Delta t} = \sqrt{2} M_0(\omega). \tag{8.174}$$

Similar we obtain for the detail filter

$$f_d(z) = \sum_{nn'} c_n (-1)^{n-1} h_{n'-n-1} z^{-n'} = \sum c_n z^{-n} (-1)^{n-1} h_{n'-n-1} z^{n-n'}. \tag{8.175}$$

Since only even values of n' are relevant, we may change the sign by $(-1)^{n'}$ to obtain

$$\sum c_n z^{-n} (-1)^{n'-n-1} h_{n'-n-1} z^{n-n'} = z^* h(-z)\, c(z) = g^*(z)\, c(z) \tag{8.176}$$

where

$$g(z) = \sum_n (-1)^{n-1} h_{-n-1}^* z^{-n} = \sum_n (-1)^{-n-2} h_n^* z^{n+1} = z \sum_n h_n^* (-z)^n$$

$$= z \left(\sum_n h_n (-z)^{-n} \right)^* = z h^*(-z). \tag{8.177}$$

8.7.2 Example: Haar Wavelet

For the Haar wavelet with[13]

$$h_0 = h_1 = \frac{1}{\sqrt{2}} \quad h_n = 0 \text{ else} \tag{8.178}$$

$$g_{-1} = \frac{1}{\sqrt{2}} \quad g_{-2} = -\frac{1}{\sqrt{2}} \quad g_n = 0 \text{ else} \tag{8.179}$$

[13]The standard form of the Haar wavelet with $g_0 = 1/\sqrt{2}$, $g_1 = -1/\sqrt{2}$ differs from (8.179) by a shift and time reversal. The resulting wavelet basis, however, is the same.

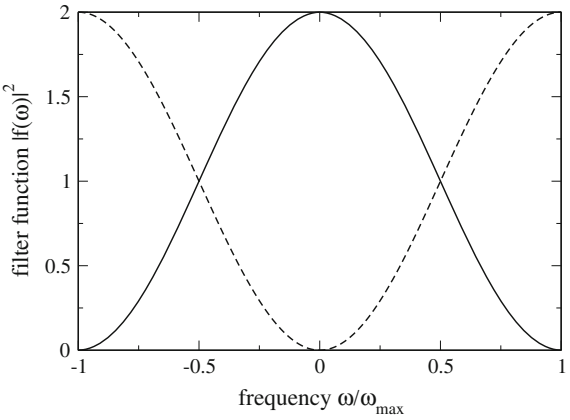

Fig. 8.20 Haar filter pair

we obtain the filter functions

$$h(z) = \frac{1}{\sqrt{2}}\left(1 + \frac{1}{z}\right) \quad g(z) = \frac{1}{\sqrt{2}}(z - z^2). \tag{8.180}$$

On the unit circle,

$$|h(\mathrm{e}^{\mathrm{i}\omega\Delta t})|^2 = 1 + \cos\omega\Delta t \tag{8.181}$$

$$|g(\mathrm{e}^{\mathrm{i}\omega\Delta t})|^2 = 1 - \cos\omega\Delta t \tag{8.182}$$

which describes a low and a high pass forming a so called quadrature mirror filter pair (Fig. 8.20) [92].

8.7.3 Signal Reconstruction

The wavelet transformation can be inverted using the expansion

$$\sum_n c_{m,n}\Phi_{m,n}(t) = \sum_n c_{m-1,n}\Phi_{m-1,n}(t) + \sum_n d_{m-1,n}\Psi_{m-1,n}(t) \tag{8.183}$$

where the coefficients at the higher level of approximation are obtained from

$$\begin{aligned} c_{m,n'} &= \sum_n c_{m-1,n} < \Phi_{m,n'}|\Phi_{m-1,n} > + \sum_n d_{m-1,n} < \Phi_{m,n'}|\Psi_{m-1,n} > \\ &= \sum_n c_{m-1,n} h_{n'-2n} + \sum_n d_{m-1,n}(-1)^{n'-1} h^*_{2n-n'-1} \\ &= \sum_n c_{m-1,n} h_{n'-2n} + \sum_n d_{m-1,n}(-1)^{n'-1} h^*_{2n-n'-1}. \end{aligned} \tag{8.184}$$

This can be formulated as upsampling and subsequent filtering. Formally, we insert zeros and define the up sampled coefficients

$$c^{\uparrow}_{2n} = c_{m-1,n} \quad c^{\uparrow}_{2n+1} = 0 \tag{8.185}$$

$$d^{\uparrow}_{2n} = d_{m-1,n} \quad d^{\uparrow}_{2n+1} = 0. \tag{8.186}$$

Then,

$$\sum_n c_{m-1,n} h_{n'-2n} = \sum_n c^{\uparrow}_{2n} h_{n'-2n} = \sum_n c^{\uparrow}_n h_{n'-n} \tag{8.187}$$

$$\sum_n d_{m-1,n} (-1)^{n'-1} h^*_{2n-n'-1} = (-1)^{n'-1} \sum_n d^{\uparrow}_{2n} h^*_{2n-n'-1}$$

$$= (-1)^{n'-1} \sum_n d^{\uparrow}_n h^*_{n-n'-1} = \sum (-1)^n d_n g_{n'-n} \tag{8.188}$$

where due to (8.186) the alternating sign can be omitted. Z-transformation then gives

$$\sum_{n,n'} c_n h_{n'-n} z^{-n'} = \sum_{n,n'} c_n z^{-n} h_{n'-n} z^{n-n'} = h(z)\, c(z) \tag{8.189}$$

$$\sum_{nn'} d_n g_{n'-n} = g(z) d(z) = z h^*(-z)\, d(z). \tag{8.190}$$

8.7.4 Example: Analysis with Compactly Supported Wavelets

Wavelet analysis has become quite popular for processing of audio and image data. In Problem 8.3 we use Daubechies wavelets [93] to analyze a complex audio signal consisting of a mixture of short tones, sweeps and noise (Figs. 8.23, 8.24). Daubechies satisfies (8.117) by taking

$$M_0(\omega/2) = \left[\frac{1}{2}\left(1 + \mathrm{e}^{-\mathrm{i}\omega/2}\right)\right]^N Q(\mathrm{e}^{-\mathrm{i}\omega/2}) \tag{8.191}$$

with a trigonometric polynomial Q. This leads to a class of compactly supported orthonormal wavelet bases, which for N = 1 include the Haar wavelet as the simplest member. For N = 2,

$$M_0(\omega/2) = \left[\frac{1}{2}\left(1 + \mathrm{e}^{-\mathrm{i}\omega/2}\right)\right]^2 \frac{1}{2}\left[\left(1 + \sqrt{3}\right) + \left(1 - \sqrt{3}\right)\mathrm{e}^{-\mathrm{i}\omega/2}\right] \tag{8.192}$$

$$= \frac{1}{8}\left[\left(1+\sqrt{3}\right) + \left(3+\sqrt{3}\right)\mathrm{e}^{-\mathrm{i}\omega/2} + \left(3-\sqrt{3}\right)\mathrm{e}^{-2\mathrm{i}\omega/2} + \left(1-\sqrt{3}\right)\mathrm{e}^{-3\mathrm{i}\omega/2}\right] \tag{8.193}$$

with the four nonzero scaling parameters

$$h_0 = \frac{\sqrt{2}}{8}(1+\sqrt{3}) \approx 0.48296 \tag{8.194}$$

$$h_1 = \frac{\sqrt{2}}{8}(3+\sqrt{3}) \approx 0.83652 \tag{8.195}$$

$$h_2 = \frac{\sqrt{2}}{8}(3-\sqrt{3}) \approx 0.22414 \tag{8.196}$$

$$h_3 = \frac{\sqrt{2}}{8}(1-\sqrt{3}) \approx -0.12941. \tag{8.197}$$

This defines the wavelet basis which is known as Daubechies 2. There are no analytic expressions for the scaling and wavelet functions available. They can be calculated numerically from the infinite product (8.116) or a corresponding (infinitely) nested convolution in real space. Figures 8.21 and 8.22 show the fast convergence.

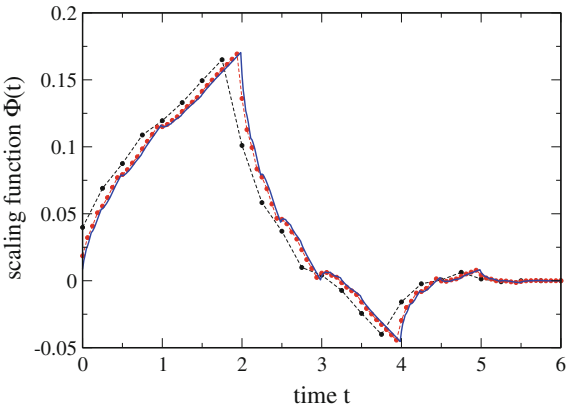

Fig. 8.21 (Daubechies 2 scaling function) The scaling function is calculated numerically in the time domain from the Fourier transform of (8.116) with a finite number of factors. The *blue curve* shows the result for $j_{max} = 7$, *red dots* show results for $j_{max} = 5$, *black dots* for $j_{max} = 3$. Delta functions are replaced by rectangular functions of equal area

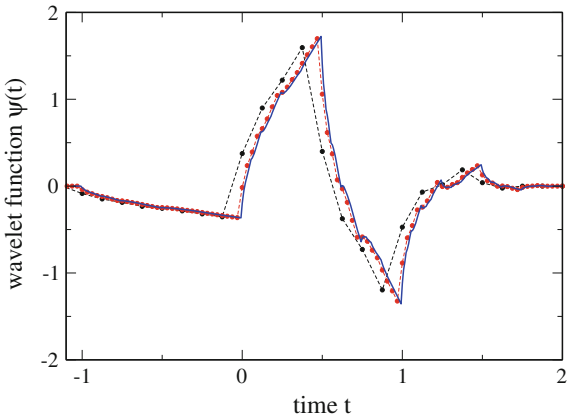

Fig. 8.22 (Daubechies 2 wavelet function) The wavelet function is calculated numerically in the time domain from the Fourier transform of (8.116) and (8.147) with a finite number of factors. The *blue curve* shows the result for $j_{max} = 7$, *red dots* show results for $j_{max} = 5$, *black dots* for $j_{max} = 3$. Delta functions are replaced by rectangular functions of equal area

Problems

Problem 8.1 Short Time Fourier Transformation

In this computer experiment STFT analysis of a frequency modulated signal

$$f(t) = \sin \Phi(t) = \sin\left(\omega_0 t + \frac{a\omega_0}{\omega_1}(1 - \cos\omega_1 t)\right) \tag{8.198}$$

with a momentaneous frequency of

$$\omega(t) = \frac{\partial \Phi}{\partial t} = \omega_0(1 + a\sin\omega_1 t) \tag{8.199}$$

is performed and shown as a spectrogram (Figs. 8.10, 8.11). Sampling frequency is 44100 Hz, number of samples 512.

You can vary the carrier frequency ω_0, modulation frequency ω_1 and depth a as well as the distance between the windows. Study time and frequency resolution

Problem 8.2 Wavelet Analysis of a Nonstationary Signal

In this computer experiment, a complex signal is analyzed with Morlet wavelets over 6 octaves (Fig. 8.14). The signal is sampled with a rate of 44 kHz. The parameter d of the mother wavelet (8.61) determines frequency and time resolution. The frequency ω_0 of the mother wavelet is taken as the Nyquist frequency which is half the sampling rate. The convolution with the daughter wavelets (8.76) is calculated at 400 times with a step size of 0.726 ms (corresponding to 32 samples)

$$t_n = t_0 + n\Delta t \tag{8.200}$$

and for 300 different values of the scaling parameter

$$s_m = 1.015^m. \tag{8.201}$$

The signal consists of two sweeps with linearly increasing frequency of the form

$$f_{1,2}(t) = \sin\left[\omega_{1,2}t + \frac{\alpha_{1,2}}{2}t^2\right] \tag{8.202}$$

and another component which switches between a 5 kHz oscillation and the sum of a 300 Hz and a 20 kHz oscillation at a rate of 20 Hz

$$f_3(t) = \begin{cases} \sin(\omega_{20kHz}t) + \sin(\omega_{300Hz}t) & \text{if } \sin(\omega_{20Hz}t) < 0 \\ \sin(\omega_{5kHz}t) & else. \end{cases} \tag{8.203}$$

Study time and frequency resolution as a function of d

Problem 8.3 Discrete Wavelet Transformation

In this computer experiment the discrete wavelet transformation is applied to a complex audio signal. You can switch on and off different components like sweeps, dial tones and noise. The wavelet coefficients and the reconstructed signals are shown. (see Figs. 8.23, 8.24).

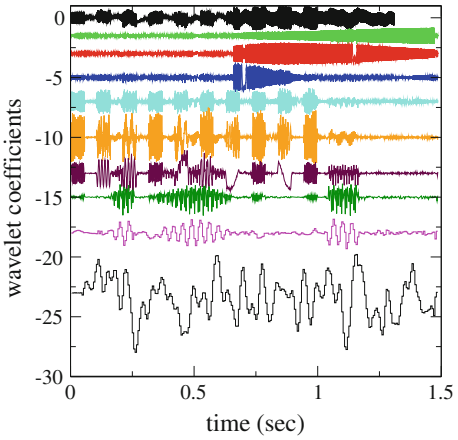

Fig. 8.23 (Wavelet coefficients of a complex audio signal) From ***Top*** to ***Bottom*** The *black curve* shows the input signal. The finest details in *light green*, *red* and *blue* correspond to a high frequency sweep from 5000–15000 Hz starting at 0.7 s plus some time dependent noise. *Cyan*, *orange* and *maroon* represent a sequence of dial tones around 1000 Hz, *dark green* and *magenta* show the signature of several rectangular 100 Hz bursts with many harmonics. The *black curve* at the ***Bottom*** shows the coefficients of the coarse approximation, which essentially describes random low frequency fluctuations. The *curves* are vertically shifted relative to each other

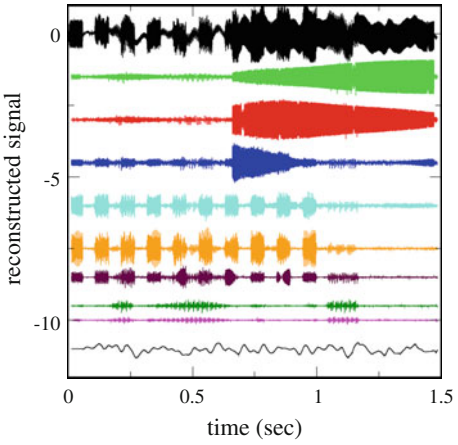

Fig. 8.24 (Wavelet reconstruction) The different contributions to the signal are reconstructed from the wavelet coefficients. Color code as in Fig. 8.23. The original signal (***Top*** *black curve*) is exactly the sum of the coarse approximation (***Bottom*** *black curve*) and all details (*colored curves*). The *curves* are vertically shifted relative to each other